Structural and functional analysis of RecJ-type exonucleases

Doctoral Thesis

2009. 3

Taisuke Wakamatsu

Graduate School of Frontier Biosciences, Osaka University

Contents

Abbreviations

3R	DNA repair, recombination and replication
BER	base excision repair
CD	circular dichroism
cd-ttRecJ	the core domain of ttRecJ
dsDNA	double-stranded DNA
ecRecJ	*E. coli* RecJ
ecSSB	*E. coli* SSB
hiRecJ	*H. influenzae* RecJ
hiSSB	*H. influenzae* SSB
IPTG	isopropyl-β-D-thiogalactopyranoside
ITC	isothermal titration calorimetry
MMR	mismatch repair
MS	mass spectrometry
pAp	3′-phosphoadenosine 5′-phosphate
PMSF	phenylmethanesulfonyl fluoride
r.m.s.d.	root mean square deviation
RNase	ribonuclease
SSB	single-stranded DNA-binding protein
SSB-Ct	C-terminal nine residues of SSB
ssDNA	single-stranded DNA
ssRNA	single-stranded RNA
ttRecJ	*T. thermophilus* RecJ
ttSSB	*T. thermophilus* SSB

General introduction

The maintenance of genomic integrity is of crucial importance for all living cells. Modifications of DNA can lead to mutations, which change the coding sequence of DNA and can lead to cancers and aging in mammals. However, organisms have DNA repair and recombination systems, which can remove the damaged lesions from DNA (Schärer, 2003, Fig. 1). Some DNA exonucleases have key roles in such systems. In prokaryotes, RecJ is a representative DNA exonuclease. RecJ has Mg^{2+}-, Mn^{2+}-dependent 5′-3′ exonuclease activity that is specific for singe-stranded DNA (ssDNA). The crystal structure of the core domain RecJ form *Thermus thermophilus* HB8 (40–433 residues; cd-ttRecJ) containing DHH motifs I–IV and DHHA1 motif in complex with the Mn^{2+} ion was determined by our group (Yamagata *et al*., 2002, Fig 2). This has been the only report detailing the RecJ structure. Cd-ttRecJ has two domains (I and II) connected by a long α-helix. The structure of cd-ttRecJ was studied, and it revealed that the conserved residues in the motifs constitute the active site—which is located in the groove between the two domains and the Mn^{2+} ion—that is essential for the exonuclease activity and is coordinated by several residues in the DHH motifs I–IV. However, the intact (full-length) structure and ssDNA-complex structure have not been determined so far. The lack of structural information has hampered the study of the mechanism of action of RecJ. Also, it has recently been reported that the ssDNA-binding protein (SSB) of *Escherichia coli* and *Haemophilus influenzae* bind to RecJ directly and enhance the RecJ exonuclease activity (Han *et al*., 2006; Sharma *et al*., 2009); however, it has not been identified whether the mechanism can be applied to ttRecJ, whose full-length structure (666 residues) is longer than that of RecJ from *E.*

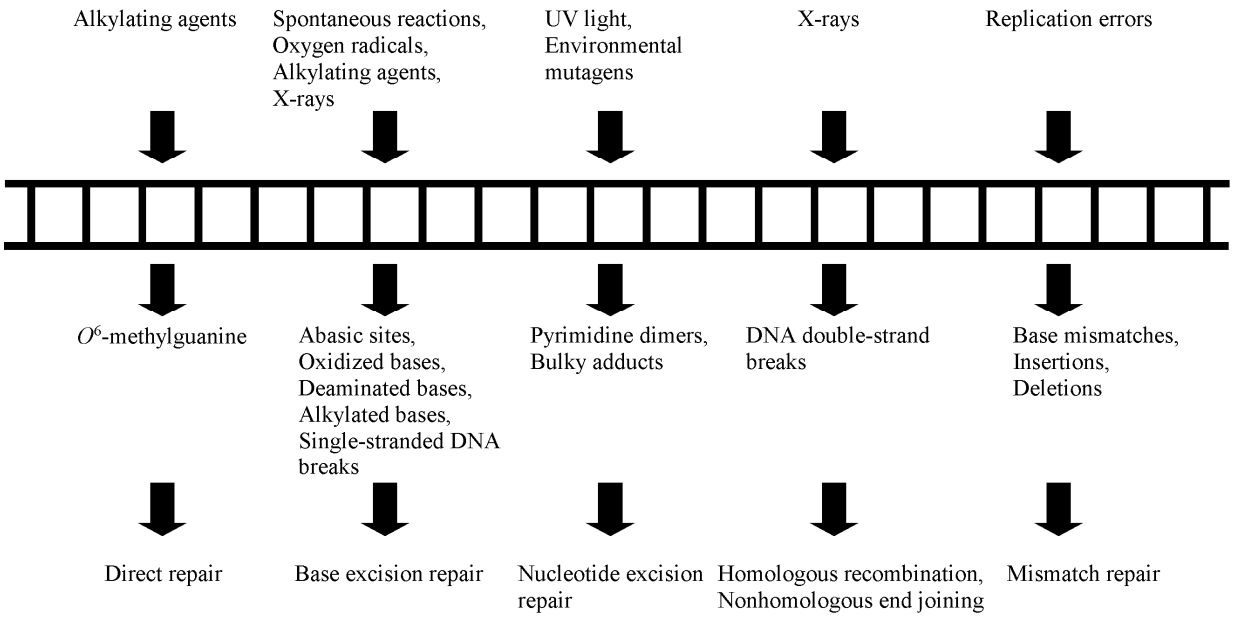

FIGURE 1. DNA-damaging agents, damaged DNA lesions, and DNA repair systems.

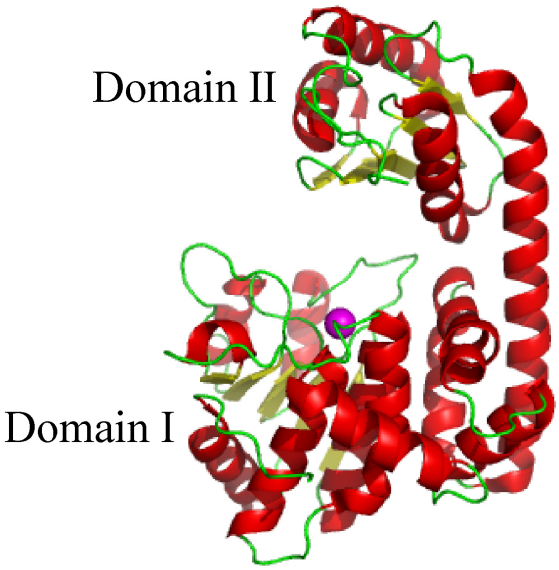

FIGURE 2. Crystal structure of cd-ttRecJ in complex with Mn^{2+} (PDB ID: 1IR6). The Mn^{2+} ion is shown as a magenta sphere.

coli (577 residues) and *H. influenzae* (575 residues). In this thesis, I have succeeded in determining the crystal structure of ttRecJ alone and that in complex with Mg^{2+} and with Mn^{2+}. Further, I have analyzed the interaction between ttRecJ and *T. thermophilus* HB8 SSB (ttSSB) in detail. These findings are stated in chapter I.

The DHH motifs I–IV are definitely present in RecJ-like family proteins. This family, also called the DHH superfamily, can be divided into two groups on the basis of a C-terminal domain (DHHA1 and DHHA2 domain) that is well conserved within each group but not across the groups. The most characteristic of these is the third motif, with the signature DHH (Asp-His-His), after which this superfamily was named (Aravind and Koonin, 1998). It is known that there are mainly three RecJ-like family I proteins (RecJ-type exonucleases), i.e., RecJ proteins (N_155469), exopolyphosphatase-related proteins (family N_142143 in bacteria, family O_155470 in archaea), and putative poly(A) polymerase (family O_142140) according to the SYSTERS database (Krause *et al*., 1999). *T. thermophilus* HB8 contains three RecJ-like family I proteins, i.e., TTHA0118 (exopolyphosphatase-related proteins), TTHA0831 (putative poly(A) polymerase), and TTHA1167 (ttRecJ) (Fig. 3A). In contrast to RecJ, study of exopolyphosphatase-related proteins belonging to RecJ-type exonuclease family has been considerably primitive. Recently, it was reported that the exopolyphosphatase-related protein YtqI from *Bacillus subtilis* hydrolyzed short-length ssRNA and 3′-phosphoadenosine 5′-phosphate (pAp) in the presence of $MnCl_2$ *in vitro* (Mechold *et al*., 2006). The *ytqI* gene was able to complement both *orn* (oligoribonuclease) and *cysQ* (pAp phosphatase) mutants in *E. coli*. However, there is no report concerning the polarity, cleavage pattern, metal ion-dependence, and enzymatic kinetics of these activities. The crystal structure of BF3670 from

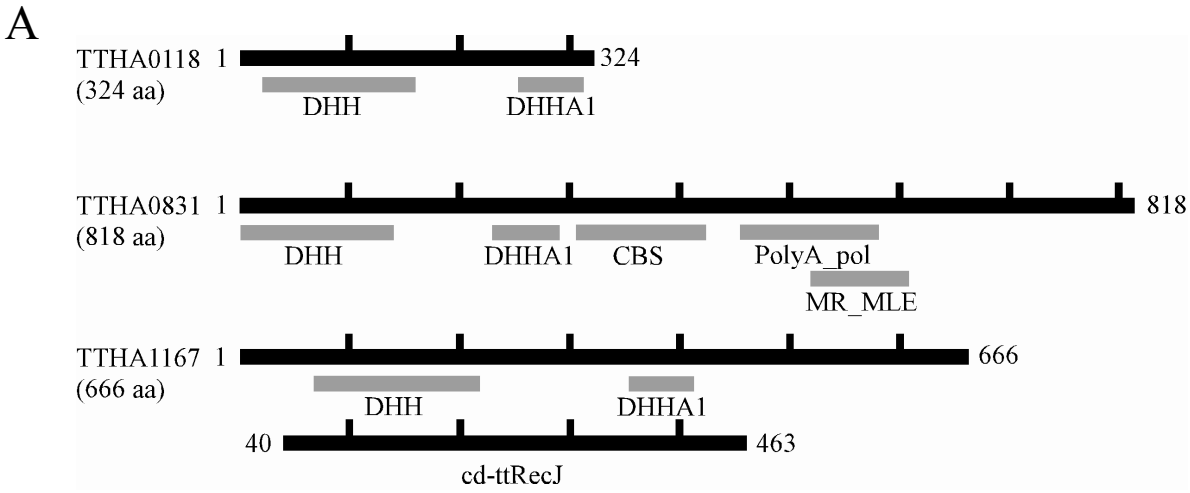

B

		Motif I		Motif II		Motif III
consensus		xxUUxxxxxDxDOUxOxUxUxxUxxxxx		xxxUUUUDxxxxxxxxxxx		xxUUUUDHHxxxx
TTHA0118	(27)	IYIATHVDPDGDAIGSSLGLYRALKALG	(31)	GATLVALDSAEPSRVVGVP	(2)	GFVINIDHHGTNP
Mpn140	(23)	IVIFHHIRPDGDCLGAQHGLARLIQTNF	(34)	QALAVIVDANYKERIECRD	(7)	KAVLRIDHHPNED
YtqI	(14)	IILHRHVRPDPDAYGSQCGLTEILRETY	(30)	GALVIVCDTANQERIDDQR	(4)	AKLMKIDHHPNED
BF3670	(23)	IVIVSHVSPDGDAIGSSLGLYHFLDSQD	(40)	ADVICCLDFNALKRIDEMS	(7)	GRKIMIDHHLYPE
ttRecJ	(72)	KRIRVHGDYDADGLTGTAILVRGLAALG	(28)	SDLFLTVDCGITNHAELRE	(5)	VEVIVTDHHTPGK
ecRecJ	(71)	TRIIVVGDFDADGATSTALSVLAMRSLG	(30)	AQLIVTVDNGISSHAGVEH	(5)	IPVIVTDHHLPGD
hiRecJ	(67)	QKIVIVGDFDADGATSTALSVLALRQLG	(30)	VQLLMTVDNGVSSFDGVAF	(5)	IRVLVTDHHLPPE
bsRecJ	(80)	EKIMIYGDYDADGVTSTSVMLHTLQKLS	(29)	FSLIITVDTGIAAVHEAKV	(5)	LDVIITDHHEPGP

		Motif IV		DHHA1 motif (RecJ-like family 1-specific motif)	
consensus		xxxxxxxxxxxxxxxxxxUUUxOUUxDxxxUxxxxx		xxxxxxxxxxxxxGGHxxOOOUxUxxx	
TTHA0118	(18)	VKDLIDLLGVEWTAEIATPVLTGILTDTGNFRFANT	(100)	GVSAQNIALKLGGGHVPAAGATLKGL	(23)
Mpn140	(19)	VVDLAVQAKWKLSPPAATALYLGIYTDSNRFLYSNT	(102)	GINVREVALKYGGGGHIQASGAVLKSK	(16)
YtqI	(21)	LYLEGKEHGWKLNTKAAELIYAGIVGDTGRFLFPNT	(103)	GPVINGLARKYNGGGHPLASGASIYSW	(18)
BF3670	(20)	RLICRMGYFSDISKEGAECIYTGMMTDTGGFTYNSN	(109)	FPCNRLAAEFFNGGGHLNASGGEFYGT	(21)
ttRecJ	(29)	LWALHERLGLPPPLEYADLAAVGTIADVAPLWGWNR	(148)	EALRSAEDLLLRYGGHKEAAGFAMDEA	(261)
ecRecJ	(43)	GWFDERNIAIPNLAELLDLVALGTVADVVPLDANNR	(168)	RLDTLYPGMMLKFGGHAMAAGLSLEED	(137)
hiRecJ	(41)	ELGIFTAETQPNFTDLLDLVALGTIADVVPLDQNNR	(168)	RIHSQHPNMILKFGGHAMAAGLSIREE	(141)
bsRecJ	(28)	AFKLAHALLGELPDELLDLAAIGTIADLVPLHDENR	(160)	ESLSECRDILPHFGGHPMAAGMTLKAE	(361)

FIGURE 3. Primary sequence of RecJ-like family I proteins. *A*, Schematic representation of sequence motifs in RecJ-like family I proteins in *T. thermophilus* HB8, i.e., TTHA0118 (exopolyphosphatase-related protein), TTHA0831 (putative poly(A) polymerase), and TTHA1167 (ttRecJ). The Pfam domain definitions are shown at the down of each sequence (Finn *et al*., 2008). The region of cd-ttRecJ is shown below TTHA1167. *B*, Amino acid sequences of exopolyphosphatase-related proteins and RecJ proteins. The amino acid sequence of TTHA0118, Mpn140, YtqI, ttRecJ, *E. coli* RecJ (ecRecJ), *H. influenzae* RecJ (hiRecJ), and *B. subtilis* RecJ (bsRecJ) are aligned according to Aravind and Koonin (1998). Shown in parentheses is the number of amino acids not shown in the alignment. Motifs with variant residues are numbered. U indicates a bulky hydrophobic residue, and O indicates a small residue. TTHA0118 (*T. thermophilus* HB8, YP_143384); Mpn140 (*M. pneumoniae* M129, NP_109828); YtqI (*B. subtilis*, AAC00337); BF3670 (*B. fragilis*); ttRecJ (*T. thermophilus* HB8, YP_144433); ecRecJ (*E. coli* ATCC 8739, YP_001723816); hiRecJ (*H. influenzae* Rd KW20, NP_439370); and bsRecJ (*B. subtilis* str. 168, NP_390640).

Bacteroides fragilis (Fig. 4, PDB ID: 3DMA), a YtqI homolog, was recently resolved. The overall structure is similar to that of cd-ttRecJ. However, the structure provides no valuable information regarding its function *in vivo*. Detailed phenotype studies of the deletion mutants of exopolyphosphatase-related proteins have been insufficient. In this thesis, I have characterized the enzyme activities of TTHA0118 from *T. thermophilus* HB8 and its deletion mutant. Further, I have characterized the enzyme activities of Mpn140, an exopolyphosphatase-related protein from *Mycoplasma pneumoniae*. These findings are stated in chapter II.

I have shown that there is a difference in the substrate specificity in RecJ-type exonucleases through these studies.

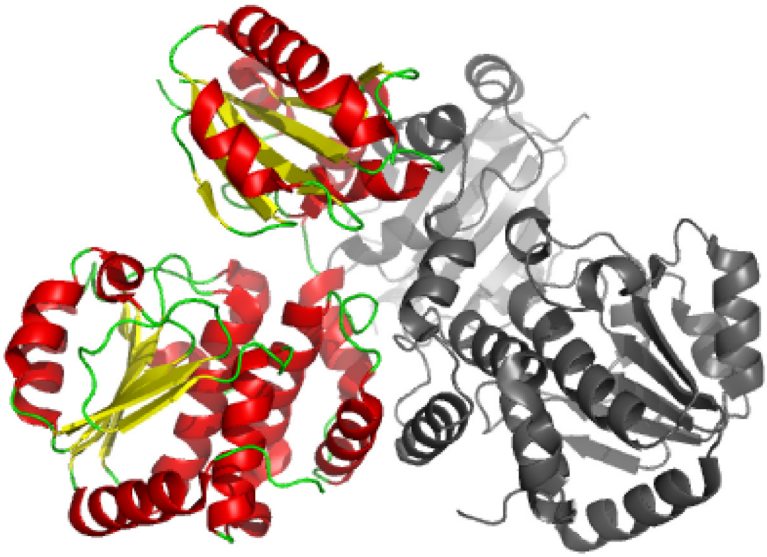

FIGURE 4. Crystal structure of BF3670 (PDB ID: 3DMA). BF3670 is a dimer.

Chapter I

Structural and functional analysis of RecJ from *Thermus thermophilus* HB8

Abstract

RecJ is single-stranded DNA (ssDNA)-specific 5′-3′ exonuclease and deoxyribophosphodiesterase (dRPase) that functions in DNA repair and recombination systems in almost bacteria and archaea. As far, our group has reported the crystal structure of the catalytic core domain of RecJ from *Thermus thermophilus* HB8 (cd-ttRecJ) containing motifs I–IV and DHHA1 motif that is bound to an Mn^{2+} ion and showed that cd-ttRecJ folded into two domains. However, the intact RecJ structure has not been reported so far. Here, I determined the 2.15–2.50 Å resolution crystal structures of the intact ttRecJ alone, in complex with Mg^{2+}, and with Mn^{2+}. The intact ttRecJ folds into three domains, and reveals that the second domain containing the DHHA1 motif is closer (~3 Å) to the first domain containing motifs I–IV than are the corresponding domains of the cd-ttRecJ structure. The DALI search and conserved residues in the oligonucleotide/oligosaccharide-binding (OB) fold suggested that the region 457–532 in the third domain was folded specifically for single-stranded DNA (ssDNA). Moreover, gel shift assay showed the region to be bound to ssDNA. In the metal ion complex, one Mg^{2+} ion and two Mn^{2+} ions coordinated with a candidate nucleophilic water molecule were found in the active site around motifs I–IV. Further, I observed that ttRecJ formed a complex with the ssDNA-binding protein from *T. thermophilus* HB8 (ttSSB) in the presence or absence of ssDNA, and ttSSB enhanced ttRecJ exonuclease activity. Together, these results suggest a possible molecular mechanism for RecJ functions.

Introduction

RecJ is a Mg^{2+}- and Mn^{2+}-dependent ssDNA-specific 5′-3′ exonuclease with processivity that in combination with deoxyribophosphodiesterase (dRPase) plays a role in homologous recombination, mismatch repair (MMR), and base excision repair (BER) (Han *et al*., 2006; Sharma and Rao, 2008; Friedberg *et al*., 1995; Lovett and Kolodner, 1989; Dianov *et al*., 1994; Kowalczykowski, 2000; Cooper *et al*., 1993; Burdett *et al*., 2001). RecJ generally degrades ssDNA unwound by UvrD and RecQ helicases in MMR and homologous recombination, respectively (Viswanathan *et al*., 2001; Courcelle and Hanawalt, 1999). In BER, RecJ is considered to remove a 5′-terminal 2′-deoxyribose-5-phosphate residue (Dianov *et al*., 1994). The orthologs of RecJ are found in almost all bacteria, and presumably, in archaea (Sutera *et al*., 1999; Aravind and Koonin, 1998; Rajman and Lovett, 2000); however, there are certain differences in their full-length proteins. For example, the full-length structures of RecJ from *T. thermophilus*, *E. coli*, *H. influenzae*, and *B. subtillus* comprise 666, 577, 575, and 786 residues, respectively.

Our group has reported the biochemical properties of the C-terminal deletion form ttRecJ and the catalytic core domain of ttRecJ (cd-ttRecJ, Fig. 2), which correspond to the region from 1 to 527 and 40 to 463, respectively; they contain motifs I–IV and the DHHA1 motif specific for the RecJ-like family I (Yamagata *et al*., 2001; Aravind and Koonin, 1998). Our group has also determined the crystal structure of cd-ttRecJ bound to a single Mn^{2+} ion (Yamagata *et al*., 2002). Cd-ttRecJ contains two domains interconnected by a long helix, and the Mn^{2+} ion is located in the groove between these domains and is coordinated by the conserved residues in motifs I–IV. The narrow

width of the groove (<14 Å) suggests that the groove binds specifically to ssDNA. Mutational analysis of RecJ from *E. coli* (ecRecJ) using crude cell extracts and complementation analysis showed that the conserved residues within motifs I–IV and the DHHA1 motif were essential for both the exonuclease activity *in vitro* and genetic function *in vivo* (Sutera *et al*., 1999). However, the intact structure of RecJ protein has not been yet reported. The cd-ttRecJ lacks 39 N-terminal and 203 C-terminal residues; the structures of these regions are therefore unknown. There is a possibility that the structure or conformation of the core domain is different from that in the full-length form.

Further, it has recently been reported that ssDNA-binding protein (SSB) bound directly and enhanced the exonuclease activity of ecRecJ and RecJ from *H. influenzae* (hiRecJ) (Han *et al*., 2006; Sharma and Rao, 2009). SSB is known to play essential roles in DNA repair, recombination, and replication (3R) in both prokaryotes and eukaryotes (Lohman and Ferrari, 1994; Wold, 1997). Thus, SSB is likely to protect ssDNA *in vivo*, directly binds to many proteins concerned with 3R processes (e.g., ExoI, RecQ, and PriA), and stimulates these activities (Lu and Keck, 2008; Shereda *et al*., 2007; Cadman and McGlynn, 2004). However, it is still uncertain whether ttRecJ interacts with SSB, which is composed of more residues (666 residues) than ecRecJ (577 resides) and hiRecJ (575 residues).

In this study, I determined the 2.15–2.50 Å resolution structures of intact ttRecJ alone, in complex with Mg^{2+}, and with Mn^{2+}. The region 457–532 formed the oligonucleotide/oligosaccharide-binding (OB) fold, and the domain actually bound to DNA. I have designated this region as the ttRecJ-OB domain in the following sections. Moreover, the results of isothermal titration calorimetry (ITC) suggested that SSB from

T. thermophilus HB8 (ttSSB) interacted with ttRecJ directly. The intact structures and analytical results concerning the interaction between RecJ and SSB needs to be available for accurately understanding the molecular mechanism of the ssDNA-specific exonuclease activity.

Experimental procedures

***Materials*:** DNA-modifying enzymes, including restriction enzymes and LA Taq polymerase, were obtained from Takara Bio Inc. Yeast extract and polypeptone were from Difco. The DNA oligomers were synthesized by BEX Co. [γ-^{32}P]ATP was from ICN. All other reagents used were of the highest commercially available grade.

***Purification of ttRecJ*:** Sequence analysis of the *T. thermophilus* HB8 genome (DDBJ/EMBL/GeneBank AB107660) identified one ORF-encoding RecJ protein. Using this sequence information, I synthesized two primers for the amplification of the target gene (*ttha1167*) by polymerase chain reaction (PCR). Amplification was carried out according to standard protocols, and the amplified gene fragment was ligated into pT7Blue T-vector (Merck) by TA cloning and confirmed by sequencing. The fragment bearing the target gene from pT7Blue-*ttha1167* was ligated into pET-11a (Merck) at the *Nde*I and *Bam*HI sites. *E. coli* Rosetta2(DE3)pLysS (Merck) cells transformed with the resulting plasmid were cultured at 37°C to 4×10^8 cells/mL in 1.5 L of LB medium containing 50 μg/mL ampicillin. The cells were then incubated for 6 h in the presence of isopropyl-β-D-thiogalactopyranoside (IPTG), harvested by centrifugation, and stored at –20°C.

All of the following procedures were carried out at room temperature unless stated otherwise. Frozen cells (30 g) were thawed, suspended in 100 mL of buffer I (50 mM Tris-HCl (pH 8.0), 50 mM NaCl, 1 mM phenylmethanesulfonyl fluoride (PMSF), and 1 mM EDTA), and disrupted by sonication on ice. The lysate was incubated at 70°C for 15 min and centrifuged (38,000 *g*) for 60 min at 4°C. Ammonium sulfate was added

to the resultant supernatant to a final concentration of 1.5 M, and loaded onto a Toyopearl Ether-650M (Tosoh) column (bed volume, 20 mL) equilibrated with buffer II (50 mM Tris-HCl (pH 8.0), 1.5 M ammonium sulfate, and 1 mM EDTA). Proteins were eluted with a linear gradient of 1.5–0 M ammonium sulfate (total volume, 250 mL). The resultant supernatant was dialyzed against buffer III (20 mM Tris-HCl (pH 8.0) and 1 mM EDTA) and loaded onto a Toyopearl SuperQ-650M (Tosoh) column (bed volume, 10 mL) equilibrated with buffer III. Proteins were eluted with a linear gradient of 0–1 M NaCl (total volume, 200 mL). Fractions containing the ttRecJ were collected and concentrated by a Vivaspin concentrator (cutoff MW, 10000). The concentrated solution was applied to a Superdex 200 HR 10/30 column (GE Healthcare Biosciences) that was equilibrated with buffer IV (20 mM Tris-HCl (pH 7.5) and 100 mM KCl) and eluted with the same buffer using an ÄKTA explorer system (GE Healthcare Biosciences). The fractions containing ttRecJ were concentrated and stored at 4°C. At each step, the fractions were analyzed by SDS-PAGE. The concentration of the purified protein was determined by using the molar absorption coefficient at 278 nm calculated according to the formula of Kuramitsu *et al*. (1990).

***Purification of ttSSB*:** Sequence analysis of the *T. thermophilus* HB8 genome (DDBJ/EMBL/GeneBank AB107660) identified one ORF-encoding SSB protein. Using this sequence information, I synthesized two primers for the amplification of the target gene (*ttha0241*) by PCR. Amplification was carried out according to standard protocols, and the amplified gene fragment was ligated into pT7Blue T-vector by TA cloning and confirmed by sequencing. The fragment bearing the target gene from pT7Blue-*ttha0241* was ligated into pET-11a at the *Nde*I and *Bam*HI sites. *E. coli*

Rosetta(DE3) cells (Merck) transformed with the resulting plasmid were cultured at 37°C to 4×10^8 cells/mL in 1.5 L of LB medium containing 50 μg/mL ampicillin. The cells were then incubated for 6 h in the presence of IPTG, harvested by centrifugation, and stored at –20°C.

All of the following procedures were carried out at room temperature unless stated otherwise. Frozen cells (30 g) were thawed, suspended in 100 mL of buffer I, and disrupted by sonication on ice. The lysate was incubated at 70°C for 15 min and centrifuged (38,000 *g*) for 60 min at 4°C. Ammonium sulfate was added to the resultant supernatant to a final concentration of 1.5 M, and loaded onto a Toyopearl Ether-650M column (bed volume, 20 mL) equilibrated with buffer II. Proteins were eluted with a linear gradient of 1.5–0 M ammonium sulfate (total volume, 250 mL). The resultant supernatant was dialyzed against buffer III and loaded onto a Toyopearl SuperQ-650M column (bed volume, 10 mL) equilibrated with buffer III. Proteins were eluted with a linear gradient of 0–1 M NaCl (total volume, 200 mL). The resultant supernatant was dialyzed against buffer III and loaded onto a Toyopearl AF-Heparin HC-650 M (Tosoh) column (bed volume, 5 mL) equilibrated with buffer III. Proteins were eluted with a linear gradient of 0–1 M NaCl (total volume, 120 mL). Fractions containing the ttSSB were collected and concentrated by a Vivaspin (cutoff MW, 5000) concentrator. The concentrated solution was applied to a Superdex 200 HR 10/30 column equilibrated with buffer IV and eluted with the same buffer using an ÄKTA explorer system. The fractions containing ttSSB were concentrated and stored at 4°C.

***Preparation of the 457–532 region of ttRecJ (ttRecJ OB domain)*:** DNA fragments

expressing the region 457–532 ttRecJ were generated by PCR using *T. thermophilus* HB8 genome as a template. Amplification was carried out according to standard protocols, and the amplified gene fragment was ligated into pT7Blue T-vector and confirmed by sequencing. The fragment bearing the target gene from pT7Blue-457–532 *ttrecj* was ligated into pET-15b (Merck) at the *Nde*I and *Bam*HI sites. *E. coli* Rosetta2(DE3)pLysS cells transformed with the resulting plasmid were cultured at 37°C to 1×10^8 cells/mL in 1.5 L of LB medium containing 50 μg/mL ampicillin. The cells were then incubated for 6 h in the presence of IPTG, harvested by centrifugation, and stored at –20°C.

All of the following procedures were carried out at room temperature unless stated otherwise. Frozen cells (15 g) were thawed, suspended in 100 mL of buffer I, and disrupted by sonication on ice. The lysate was centrifuged (38,000 *g*) for 60 min at 4°C. The result supernatant was loaded onto a Ni-NTA His-Bind resin (Merck) column (bed volume, 5 mL) equilibrated with buffer V (20 mM Tris-HCl, 500 mM NaCl, and 5 mM imidazole, pH 8.0). Proteins were eluted with a linear gradient of 0.06–1 M imidazole (total volume, 100 mL). The resultant supernatant was dialyzed against buffer VI (20 mM Tris-HCl, 100 mM KCl, and 20 mM EDTA) and the His_6-tag was cleaved with thrombin (Merck); thus, only GSHM residues remained in the N-terminal of 457–532 ttRecJ. The solution was loaded onto a Ni-NTA His-Bind resin column (bed volume, 5 mL) equilibrated with buffer V to remove the His_6-tag. Ammonium sulfate was added to the flow-through fraction to a final concentration of 1.8 M, and loaded onto a Toyopearl Butyl-650M column (Tosoh) (bed volume, 5 mL) equilibrated with buffer VII (20 mM Tris-HCl (pH 8.0), 1.8 M ammonium sulfate, and 1 mM EDTA). Proteins were eluted with a linear gradient of 1.8–0 M ammonium sulfate

(total volume, 100 mL). Fractions containing the target protein were collected and stored at –4°C. This protein fragment was adsorbed onto a membrane of the Vivaspin centrifugal concentrator; therefore, the protein solution could not be concentrated by ultrafiltration.

***Spectroscopic analysis*:** Circular dichroism (CD) spectra in the far-UV region (200 nm to 250 nm) were obtained at 25°C with a Jasco spectropolarimeter, J-720W, using 1.25 μM ttRecJ in 50 mM potassium phosphate and 100 mM KCl (pH 7.5). Thermostability was investigated by recording the molar ellipticity at 222 nm from 25°C to 95°C under the same conditions as above.

***Size exclusion chromatography*:** The enzyme (50 μM) was applied onto the Superdex 200 HR 10/30 column and eluted with buffer II with a flow rate of 0.5 mL/min by the ÄKTA system. The apparent molecular weight was estimated by comparing its retention time with those of molecular weight markers (Sigma).

***Crystallization*:** Crystallization conditions for ttRecJ were surveyed by the hanging-drop vapor-diffusion method with Crystal Screen Kits (Hampton Research: Crystal Screen, Crystal Screen2, Crystal Screen Cryo, Crystal Screen Lite, Natrix, Index, Salt RX, and MembFac) at 293 K. The initial protein concentration was 10 mg/mL in 20 mM Tris-HCl (pH 7.5) and 100 mM KCl, and 1 μL of the protein solution was mixed with the same volume of reservoir solution and equilibrated against the reservoir solution. After further optimization, crystals suitable for X-ray diffraction were obtained in an optimized condition containing 0.1 M lithium sulfate monohydrate, 0.1

M N-(2-acetamido) iminodiacetic acid (pH 6.5), 12% w/v polyethylene glycol 4000, and 2% (v/v) 2-propanol at 20°C.

***Data collection, molecular replacement, model building, and refinement*:** The crystals were soaked in cryoprotective solution containing 20% glycerol and flash-cooled in a nitrogen stream (93 K). Data were collected under cryo-conditions at the beamline BL26B2 at SPring-8. Crystals of Mg^{2+}- and Mn^{2+}-complexes were prepared by soaking the crystals in the reservoir solution containing 10 mM $MgSO_4$ and 10 mM $MnSO_4$, respectively. Diffraction images were processed with the HKL2000 program (Otwinowski and Minor, 1997). Assuming that an asymmetric unit contained one subunit, the V_M and V_{sol} values (Matthews, 1968) were approximately 2.95 $Å^3Da^{-1}$ and 0.58, respectively. The regions of 49–292 and 326–433 residues of cd-ttRecJ (PDB ID: 1IR6) were applied as a search model, and the program MOLREP (Vagin and Teplyakov, 1997) was used for molecular replacement phase determination. The initial model was built with the aid of the amino acid sequence using the program PHENIX (Adams *et al*., 2002), refined with the Xtalview (Jones *et al*., 1991) and CNS programs (Brünger *et al*., 1998). The success of model refinement was evaluated at each stage by the free R factor and by inspection of stereochemical parameters with the program PROCHECK (Laskowski *et al*., 1993). The final refinement indicated that more than 85% of the residues (expect for the glycine and proline residues) fell into the most favored regions in the Ramachandran plot.

Data for the crystals of the Mg^{2+}- and Mn^{2+}-complexes were collected at a wavelength of 1.00000 Å and 1.70000 Å at the beamline BL26B2 at SPring-8. Diffraction images were processed with the HKL2000 program. The structures were

determined by molecular replacement using the intact ttRecJ alone as a starting model and refined by the CNS program. Figures were made with the programs CCP4 (Collaborative Computational Project, 1994) and Pymol (DeLano Scientific; http://www.pymol.org).

***Atomic coordinates*:** The atomic coordinates and structure factors have been deposited in the Protein Data Bank (PDB) with accession codes 2ZXO, 2ZXP, and 2ZXR.

***Assay for exonuclease activity*:** The oligo(deoxy)ribonucleotides that were used as substrates are shown in Table 1. These custom-synthesized oligo(deoxy)ribonucleotides obtained from BEX, were used as substrates for exonuclease activity assays. Such ssDNA was radiolabeled at the 5′-end with [γ-^{32}P]ATP using polynucleotide kinase. The reaction mixture (10 μL)—which contained 50 mM HEPES, 100 mM KCl, 5 mM $MgCl_2$, 10 nM 5′-^{32}P-labeled ssDNA, various concentrations of cold ssDNA, and 2.5 nM ttRecJ (pH 7.5)—was incubated at 37°C. For each time point, the reaction was quenched by the immediate addition of 1 μL of 100 mM EDTA and 11 μL of phenol/chloroform. The samples were centrifuged, and an equal volume of sample buffer (5 mM EDTA, 80% deionized formamide, 10 mM NaOH, 0.1% bromophenol blue, and 0.1% xylene cyanol) was added to the supernatant. The samples were denatured at 95°C for 3 min, and were loaded onto a 25% (w/v) acrylamide gel containing 8 M urea and 1 × TBE buffer (89 mM Tris-borate and 2 mM EDTA), and then electrophoresed in 1 × TBE buffer (Yamagata *et al*., 2001). The gel was dried and placed in contact with an imaging plate. The bands were

TABLE 1. Oligonucleotides used in the exonuclease assays.

Substrate	Sequence
DNA	
3f:	5′-ATG-3′
6f	5′-ATGACA-3′
11f	5′-ATGACAACTAA-3′
21f	5′-ATGACAACTAAAGCAACACCC-3′
33f	5′-ATGACAAAAGCAACACCCAAAACAACTCCC-3′
21r	5′-GGGTGTTGCTTTAGTTGTCAT-3′
27r	5′-GGGAGTTGTTTTGGGTGTTGCTTTAGT-3′
RNA	
3fR	5′-AUG-3′
6fR	5′-AUGACA-3′
11fR	5′-AUGACAACUAA-3′
21fR	5′-AUGACAACUAAAGCAACACCC-3′

visualized and analyzed using a BAS2500 image analyzer (Fuji Photo Film).

The percentage of undegraded ssDNA was plotted for each incubation period. Since the plot showed a linear region, the initial rate of the reaction could be obtained. In this assay, the substrate was mixed with a large excess of the enzyme. Assuming that the enzyme and substrate reacted according to a scheme similar to the Michaelis-Menten mechanism, the second step (k_{app}) was considered to be the rate-limiting step when the enzyme-bound intermediate was in the steady state. The initial rate was plotted against the concentration of substrate. The data were fitted to the Michaelis-Menten equation, and the kinetic constant was calculated by the software Igor Pro 3.14 (WaveMetrics).

Further, exonuclease activity in the presence of various divalent cations was measured. The reaction mixture (10 μL) contained 50 mM HEPES, 100 mM KCl, 5 mM divalent cation ($MgCl_2$, $MnCl_2$, $CaCl_2$, $CoCl_2$, or $ZnCl_2$), 10 nM 5′-^{32}P-labeled ssDNA, and 2 nM ttRecJ (pH 7.5) and was incubated at 37°C.

In other nuclease assays performed to confirm whether ttSSB stimulated ttRecJ activity, 40 nM ttSSB was allowed to bind to 10 nM 5′-^{32}P-labeled ssDNA for 10 min at 37°C prior to the addition of 0.5 nM ttRecJ. Custom-synthesized ssDNA, 60-mer (5′-CCGCTACCAGTGATCACCAATGGATTGCTAGGACATCTTTGCCCACCTGC AGGTTCACCC-3′) obtained from BEX, was used in this assay.

***Gel shift assay*:** Custom-synthesized ssDNAs, 21-mer (21f in Table 1) and 60-mer, 21-bp dsDNA (21f-21r in Table 1), or 21-mer ssRNA (21fR in Table 1), obtained from BEX, were used as substrates for gel shift assays. To analyze the interaction between intact ttRecJ or N-terminal GSHM addition from the ttRecJ-OB domain and

oligo(ribo)nucleotides, the reaction mixture (10 μL) containing 50 mM Tris-HCl (pH 7.5), 100 mM KCl, 20 mM EDTA, 10 nM 5′-^{32}P-labeled oligonucleotide, and 0–400 nM enzyme was incubated at 37°C. To analyze the interaction between ttRecJ and ttSSB in the presence of ssDNA, the reaction mixture (10 μL) containing 50 mM Tris-HCl (pH 7.5), 100 mM KCl, 20 mM EDTA, 10 nM 5′-^{32}P-labeled ssDNA, 40 nM ttSSB, and 0–400 nM ttRecJ was incubated at 37°C. A native PAGE loading dye (8.3 mM Tris-HCl (pH 7.5), 17 mM KCl, 5% glycerol, 0.033% BPB, and 0.033% xylene cyanol) was added to the mixture, loaded onto a 9% (w/v) or 6% (w/v) polyacrylamide gel, and electrophoresed in 1 × TBE buffer. The gel was dried and placed in contact with an imaging plate. The bands were visualized and analyzed using a BAS2500 image analyzer.

***Isothermal titration calorimetry*:** ITC experiments were performed using a VP-ITC calorimeter (MicroCal Inc.). Titration of ttSSB (5 μM, sample cell 1.417 mL) with ttRecJ (50 μM, syringe 250 μL) was analyzed at 25°C in 20 mM Tris-HCl and 100 mM KCl, pH 7.5. All samples and buffer solutions were degassed at room temperature prior to use. Briefly, injections of 10 μL of ttRecJ were added using a computer-controlled 250-μL microsyringe. The ITC data were analyzed with Origin software version 7.0 to obtain the following thermodynamic parameters: stoichiometry (N), dissociation constant (K_d), and changes in the enthalpy, entropy, and free energy of association (ΔH, ΔS, and ΔG, respectively).

Results

***Preparation of ttRecJ*:** The *ttrecj* gene encodes a protein of 666 residues (Figs. 1 and 5) and has a calculated molecular mass of 72.9 kDa with a theoretical pI of 5.9. ttRecJ was overexpressed in the soluble fraction in *E. coli* under the control of an IPTG-inducible T7 promoter. The protein was purified to homogeneity by using three-step column chromatography (Fig. 6A, lane 3). The purified protein was identified to be ttRecJ by matrix-assisted laser desorption ionization time-of-flight mass spectrometry (MALDI-TOF MS) with an overall MOWSE score of 300. Approximately 10 mg of ttRecJ was obtained from 30 g of cells. The final preparation of ttRecJ had an A_{280}/A_{260} ratio of 1.53, which suggested that the ttRecJ solution was not contaminated with any nucleotides. Size exclusion chromatography revealed that ttRecJ was eluted as a single peak with an apparent molecular mass of 98 kDa (Fig. 6B). This result indicated that ttRecJ existed in a monomer state in solution. The far-UV (200–250 nm) CD spectrum suggested that ttRecJ have a α/β or α+β fold (data not shown). ttRecJ was stable up to 80°C at pH 7.5 (data not shown).

***5′-3′ exonuclease activity of ttRecJ*:** Exonuclease activity was analyzed with 5′-end-labeled ssDNA. The reaction of ttRecJ with the labeled 11-mer ssDNA (11f in Table 1) in the presence of $MgCl_2$ gave only one radioactive band as a product on the gel (lanes 7–8 in Fig. 7). This small-sized band corresponded to the labeled mononucleotide (1-nt), which was released from the 5′-end of the substrate. Thus, intact ttRecJ exhibited high 5′-3′ exonuclease activity for ssDNA in the presence of 5

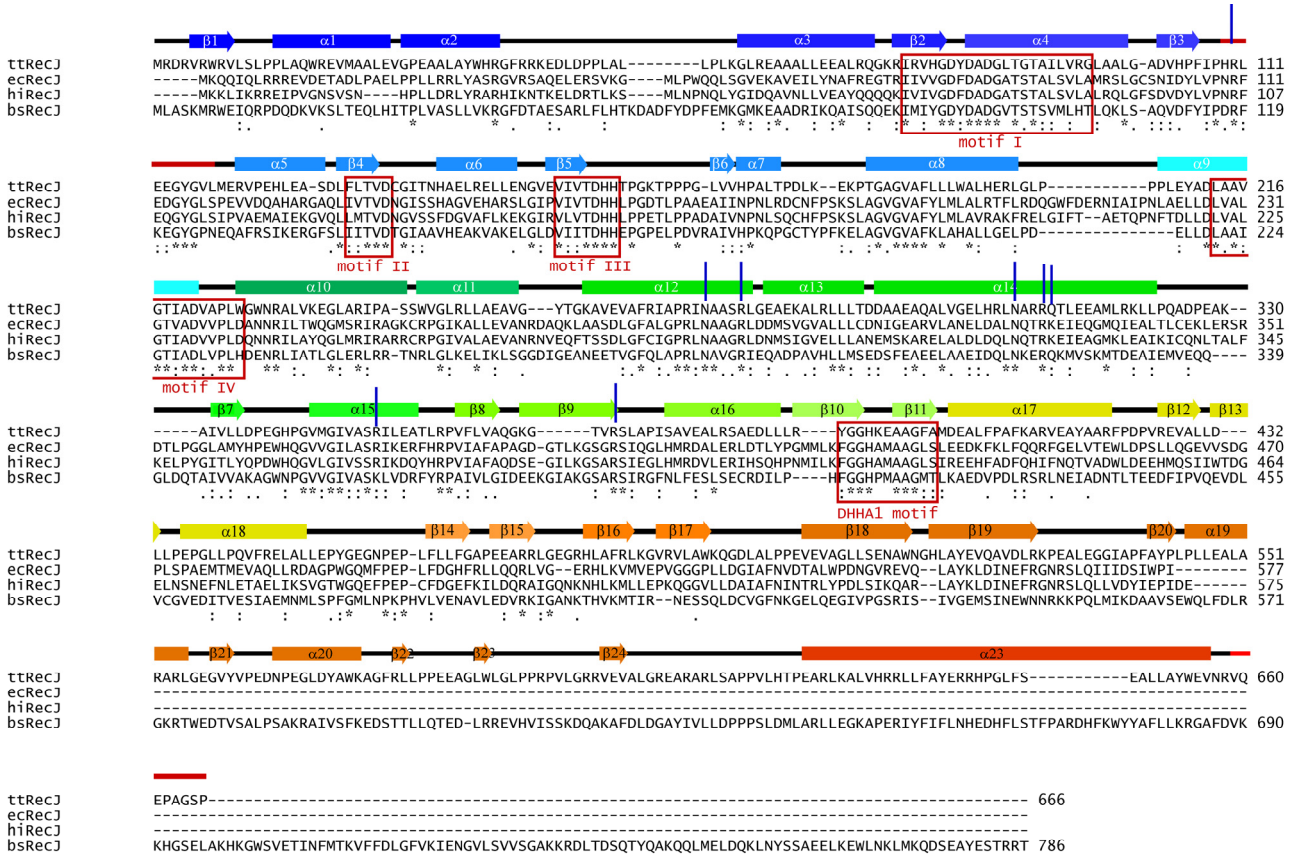

FIGURE 5. Secondary structures and sequence alignment. Shown here is the amino acid sequence alignment of ttRecJ and its homologs. The secondary structures of ttRecJ are shown above the sequences; the horizontal bars indicate α-helices and arrows indicate β-strands. Red lines indicate disordered regions. The five motifs proposed by Aravind and Koonin (1998) are designated by red boxes. Sequences shown here are as follows: ttRecJ (*T. thermophilus* HB8), ecRecJ (*E. coli*), hiRecJ (*H. influenzae*), and bsRecJ (*B. subtilis*). The sequence alignment was prepared with ClustalW (Thompson *et al*., 1994).

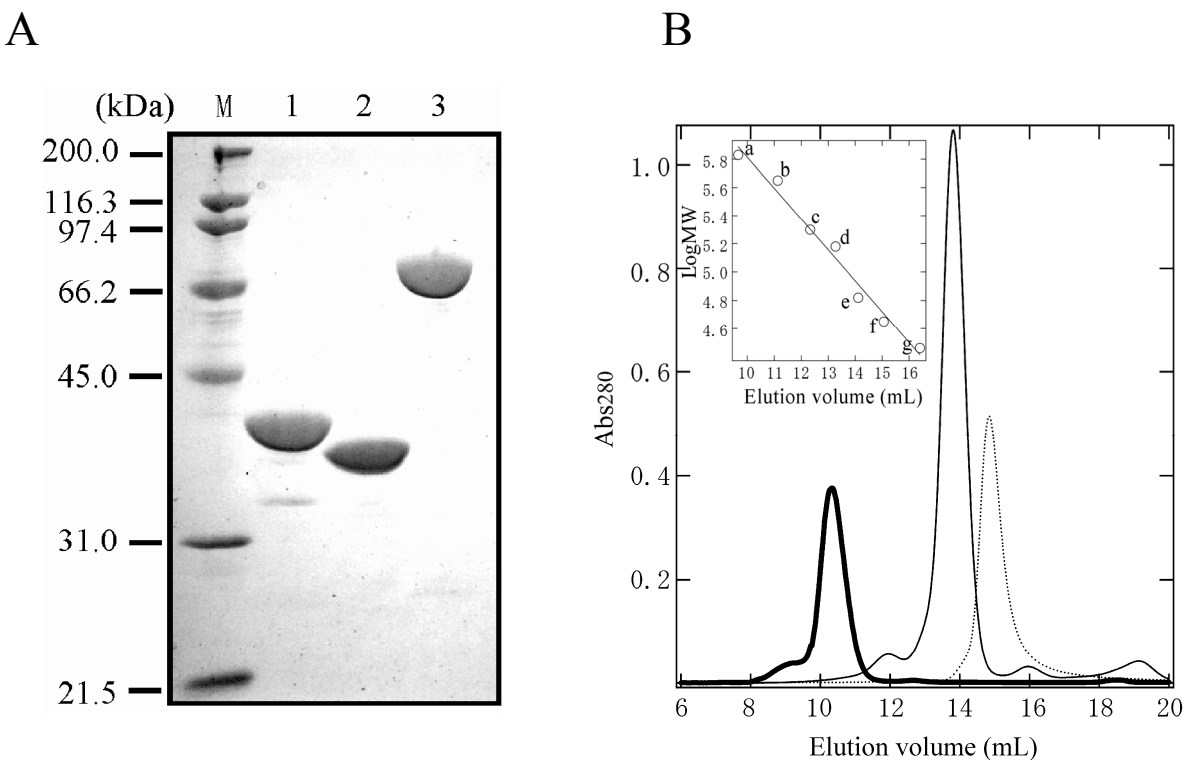

FIGURE 6. Purification of TTHA0118, Mpn140, and ttRecJ. *A*, 12.5% polyacrylamide SDS gel electrophoresis of purified protein samples. M, marker; lane 1, TTHA0118; lane 2, Mpn140; lane 3, ttRecJ. *B*, Size exclusion chromatography of TTHA0118, Mpn140, and ttRecJ. TTHA0118, Mpn140, and ttRecJ were loaded onto a Superdex 200 HR 10/30 and eluted with 20 mM Tris-HCl (pH 7.5) and 100 mM KCl. They were analyzed by absorbance at 280 nm with a flow rate of 0.5 mL/min. The inset of Fig. 6B shows a calibration curve using the molecular size markers: *a*; thyroglobulin (669 kDa), *b*; apoferritin (443 kDa), *c*; beta-amylase (200 kDa), *d*; yeast alcohol dehydrogenase (150 kDa), *e*; bovine serum albumin (66 kDa), *f*; chicken egg white albumin (44 kDa), and *g*; bovine carbonic anhydrase (29 kDa). Thick line, TTHA0118; dashed line, Mpn140; and thin line, ttRecJ.

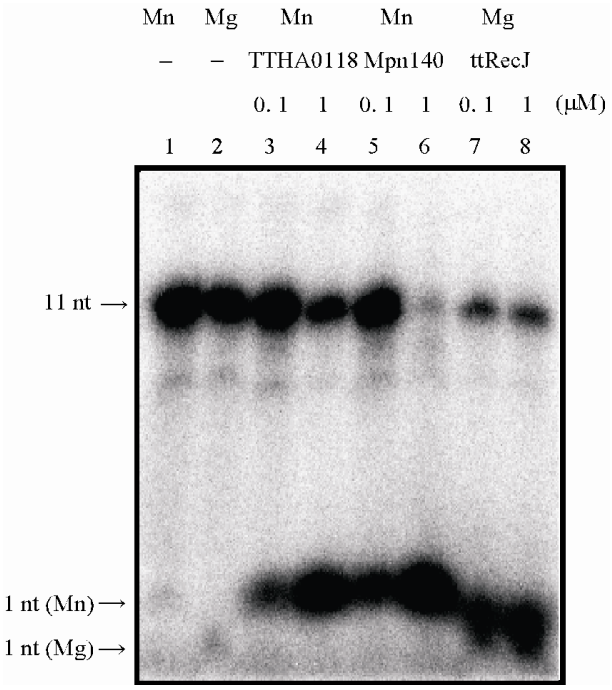

FIGURE 7. Exonuclease activity of TTHA0118, Mpn140, and ttRecJ. An aliquot of 10 nM 5′-^{32}P-labeled 11-mer ssDNA was reacted with 0.1 or 1 μM TTHA0118, Mpn140, or ttRecJ for 30 min at 37°C. The reaction mixture contained 50 mM HEPES, 100 mM KCl, 5 mM $MnCl_2$ (TTHA0118 and Mpn140) or 5 mM $MgCl_2$ (ttRecJ) (pH 7.5). Lane 1, 5 mM $MnCl_2$; lane 2, 5 mM $MgCl_2$; lanes 3–4, 0.1 or 1 μM TTHA0118; lanes 5–6, 0.1 or 1 μM Mpn140, lanes 7–8, 0.1 or 1 μM ttRecJ. The 11 nt arrow indicates the substrate 11-mer ssDNA; and the 1 nt arrow, the released 5′-end mononucleotide.

mM $MgCl_2$ at 37°C. The kinetic constants are shown in Table 2. ttRecJ showed similar kinetic constants for tested substrates.

Among the divalent cations tested (each at 5 mM), Mg^{2+} was the most effective for inducing 5′-3′exonuclease activity. The presence of Mn^{2+}, Co^{2+}, and Zn^{2+} resulted in only approximately 65%, 59%, and 2%, respectively, of the activity observed in the presence of Mg^{2+}. No activity was observed in the presence of Ca^{2+} and without metal ions.

***Overall Structure of ttRecJ*:** The three-dimensional structure of intact ttRecJ was determined by X-ray crystallography as described under "Experimental procedures". Crystals of the ligand-free enzyme, the Mg^{2+}-complex, and the Mn^{2+}-complex were obtained. The structures were determined up to 2.15–2.50 Å resolution by the molecular replacement method. Data collection, phasing, and refinement statistics are shown in Table 3. This is the first report of the three-dimensional structure of a full-length RecJ. The regions of 109–118 and 659–666 residues in the ligand-free and the Mn^{2+}-bound forms and 109–118, 138–151, 163–170, and 659–666 residues in the Mg^{2+}-bound form were disordered (Fig. 5). The average B-factors of the regions 119–128, 138–151, and 163–170 were high (~70) in the ligand-free and the Mn^{2+}-bouund forms although these residues were not disordered. Furthermore, residues in motifs I–IV underwent conformational and directional changes of the side chains. Except for these regions, the structures of ttRecJ did not undergo a large conformation change upon binding to a metal ion.

Crystals of ttRecJ contain one subunit in the asymmetric unit (Fig. 8). The overall structure of ttRecJ is comprised of twenty-three α-helices and twenty-four β-strands

TABLE 2. Kinetic constants for the exonuclease activity of ttRecJ.

Assays were performed at pH 7.5 as described under "Experimental procedures".

Substrate	K_m (μM)	k_{cat} (s^{-1})	k_{cat}/K_m ($M^{-1}s^{-1}$)
6f	1.7×10^{-1}	2.0×10^{-2}	1.2×10^{5}
11f	8.4×10^{-2}	1.2×10^{-2}	1.4×10^{5}
21f	3.7×10^{-2}	4.7×10^{-3}	1.3×10^{5}

[a] K_m and k_{cat} were determined from a nonlinear regression analysis. Substrates are shown in Table 1.

TABLE 3. Data collection and refinement statistics.

Data sets		ttRecJ (free)	ttRecJ-Mg^{2+} (complex)	ttRecJ-Mn^{2+} (complex)	
Wavelength (Å)		1.000000	1.000000	1.000000	1.700000
Resolution (Å)		50–2.50 (1.90–2.50)	50–2.15 (1.76–2.15)	50–2.30 (1.73–2.30)	50–2.65 (2.74–2.65)
Space group			$P4_32_12$		
Cell constants (Å)	*a*	83.0	83.4	83.1	83.2
	b	83.0	83.4	83.1	83.2
	c	249.2	251.1	249.9	250.3
	$\alpha = \beta = \gamma$	90°	90°	90°	90°
Data collection					
Observed reflections		1,901,745	3,511,042	2.713,119	527,198
Unique reflections		409,722	837,996	538,276	209,758
Completeness (%)		100 (99.9)	98.5 (86.0)	100 (100)	99.9 (99.5)
$I/\sigma(I)$		45.4 (6.2)	47.2 (3.3)	50.6 (9.0)	38.5 (5.0)
R_{merge} (%)[a]		7.0 (30.2)	6.4 (27.6)	7.8 (33.9)	32.2 (6.6)
Refinement					
R-factor (%)[b]		0.230	0.235	0.232	-
R_{free} (%)[c]		0.282	0.279	0.281	-
Average B factor ($Å^2$)		42.8	34.9	37.0	-
Model[d]					
Amino acids		648	616	648	-
Ligand		-	1 Mg^{2+}	2 Mn^{2+}	-
Water		180	290	293	-
Total atoms		5202	5068	5317	-
Stereochemistry[e] r.m.s d.[f]					
Bond lengths (Å)		0.011	0.011	0.011	-
Angles (°)		1.7	1.7	1.6	-

[a] Values in parentheses are for the outermost shell.

[b] $R_{merge} = \Sigma_{hkl}\ \Sigma_i|I_i(hkl)-I(hkl)|/\Sigma_{hkl}\Sigma_i I_i(hkl)$, where $I_i(hkl)$ is the observed intensity and $I(hkl)$ is the averaged intensity for multiple measurements.

[c] *R*-factor $= \Sigma||F_{obs}| - |F_{calc}||/\Sigma|F_{obs}|$

[d] R_{free} is monitored with 10% of the reflection data excluded from refinement.

[e] The asymmetric unit has one subunits.

[f] Over 85% of main-chain dihedrals fall within the "most favored regions" of the Ramachandran plot.

A

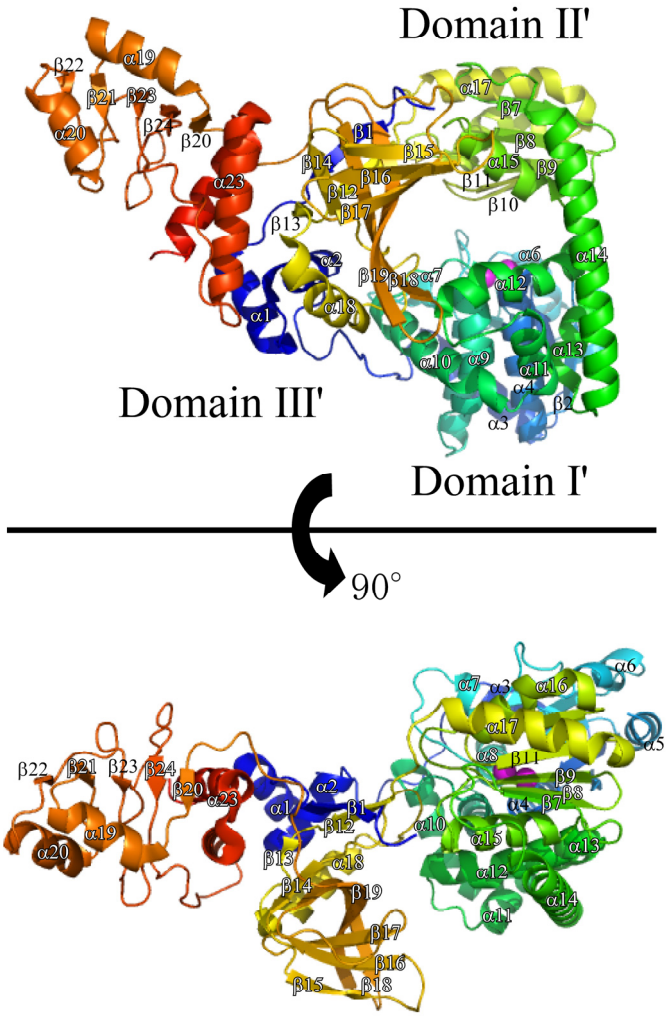

B

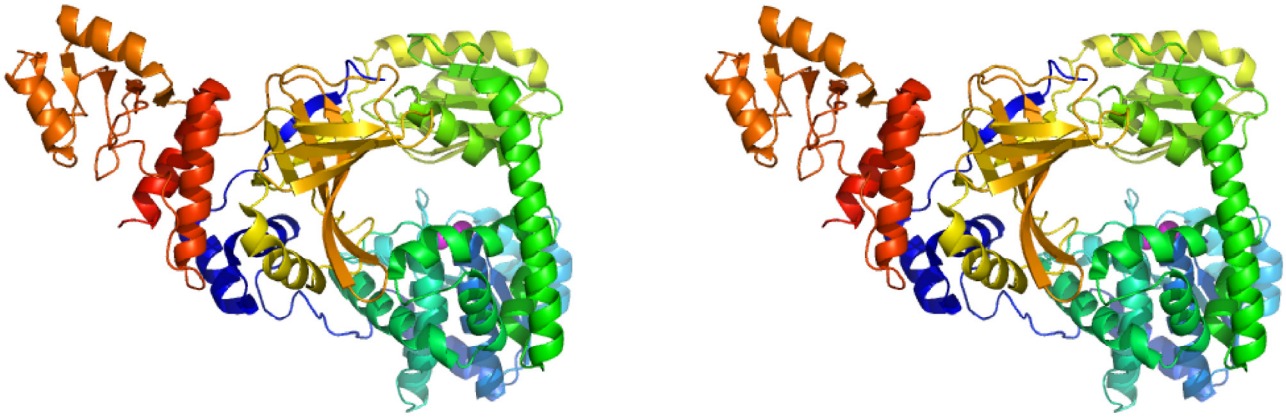

C

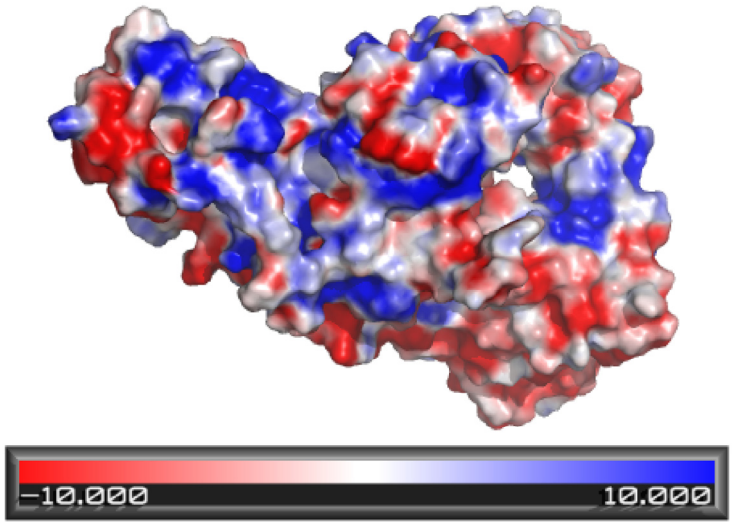

FIGURE 8. Overall structure of ttRecJ. *A*, A ribbon model of the overall structure of the ttRecJ in complex with Mn^{2+}. The color scheme for each segment is the same as that in Fig. 5. *B*, Stereoview ribbon diagram of the overall structure of the ttRecJ in complex with Mn^{2+}. *C,* An electrostatic potential map of the overall structure of the ttRecJ in complex with Mn^{2+}. Electrostatic potential was calculated using PyMOL and APBS (Baker *et al*., 2001). Mn^{2+} ions are shown in magenta spheres. The hole is formed by domains I′–III′.

(Figs. 5, 8A, and 8B). ttRecJ consists of mainly three domains: domain I′, II′, and III′. I added the prime (′) to the domain names of ttRecJ because the names of "domain I" and "domain II" have already been used in the cd-ttRecJ structure by Yamagata *et al*. (2002). The hole between these three domains is approximately 11 Å wide (Fig. 8C) and the width is shorter than that of the groove in cd-ttRecJ (14 Å). This hole is too narrow for binding to dsDNA because the theoretical diameter of dsDNA is 20 Å. Domain I′ and II′ are connected by a long α-helix (α14). The structures of domains I′ and II′ are almost identical to the corresponding domains (domains I and II in Fig. 2) of cd-ttRecJ with a root mean square deviation (r.m.s.d.) of 2.53 Å for the same Cα atoms. Domain III′ consists of the residues from N- and C-terminal regions and is connected with domain I′ and II′ by a loop composed of Arg38–Lys56 and Phe421–Val425, respectively. Overall, domain II′ that includes the DHHA1 motif is nearer to domain I′ that includes motifs I–IV than the same domains of cd-ttRecJ probably because of the presence of domain III′ (Fig. 9). The distance between His394 in the DHHA1 motif and the Mn^{2+} ion in the same position in the intact structure and cd-ttRecJ are approximately 10 Å and 14 Å, respectively.

***The OB-fold domain in domain III′*:** Interestingly, the regions of 457–532 residues in domain III′ of all ttRecJ structures determined in this study formed oligonucleotide/oligosaccharide-binding (OB) folds (Murzin, 1993), consisting of five β-strands (β15–19 in Figs. 5, 8, and 10). This region extrudes from the catalytic core domain and forms a structural domain separate from the rest of the domain III′. Therefore, I have designated this region as the ttRecJ-OB domain. The DALI search with this domain revealed many candidates with a Z-score above 4.0 and r.m.s.d. below

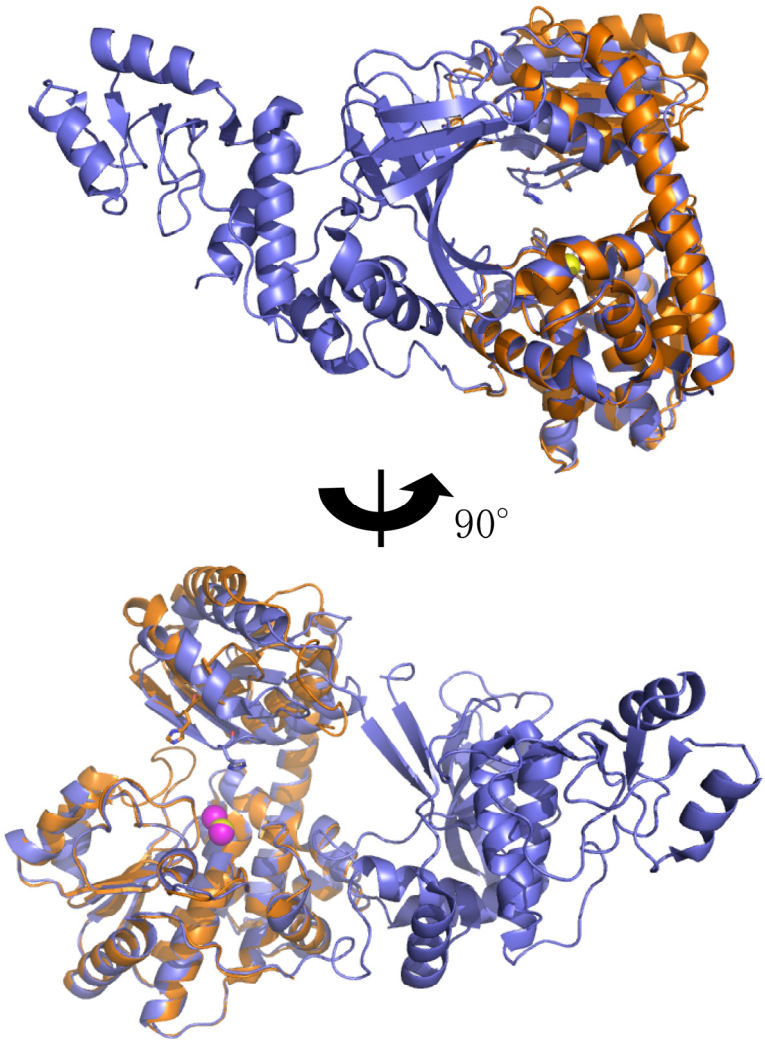

FIGURE 9. Superimposition of the intact structure (blue) and cd-ttRecJ (orange). The figure was produced with the LSQKAB program. Mn^{2+} ions in the intact structure are shown in magenta spheres. Mn^{2+} ion in cd-ttRecJ is shown in yellow spheres. His394 in the DHHA1 motif is shown in the stick form.

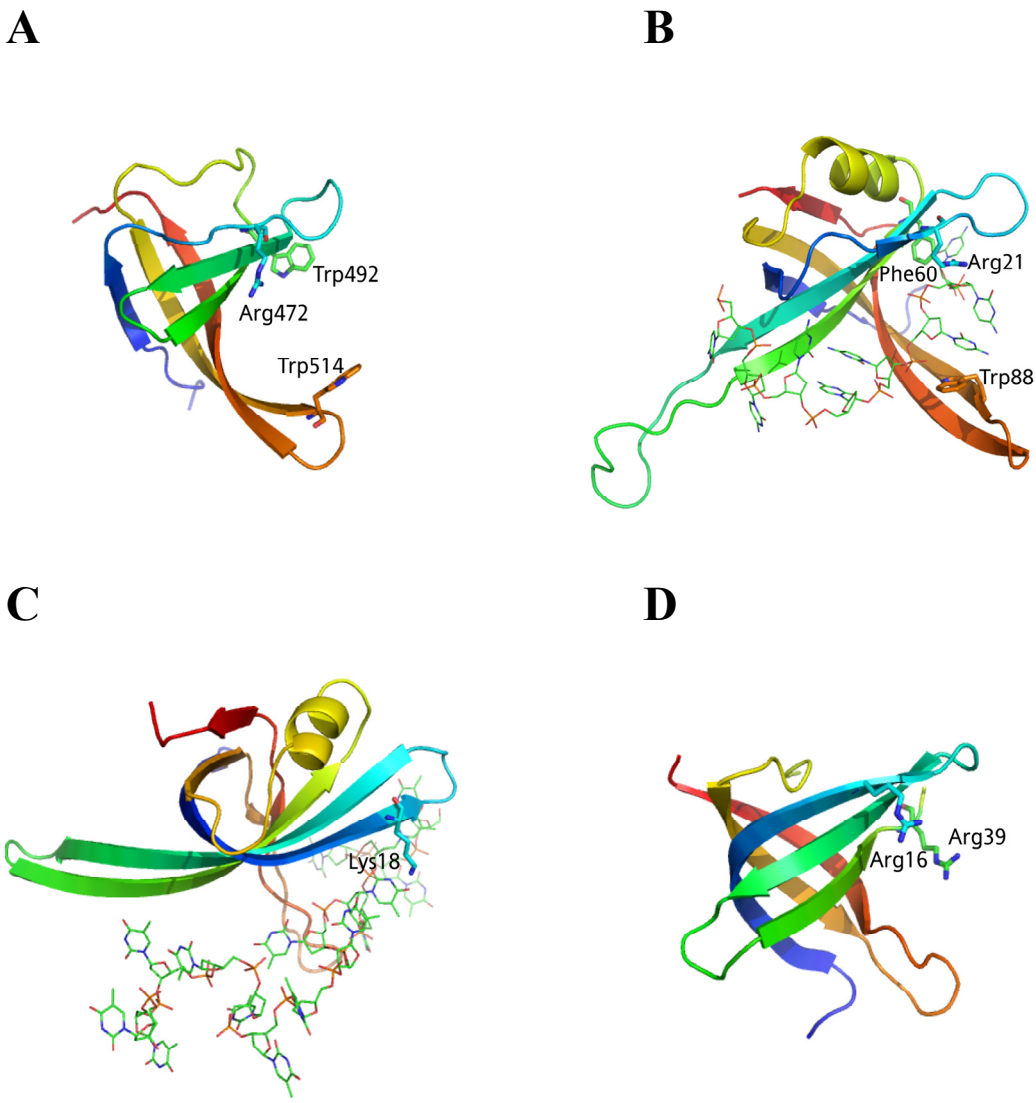

FIGURE 10. Structural comparison between some aligned OB domains. *A,* the region of 457–532 ttRecJ (PDB ID: 2ZXP). *B,* the region of 1–112 ecSSB (PDB ID: 1EYG). *C,* the region of 1–102 of *E. coli* PriB (PDB ID: 2CCZ). *D,* the region of 2–79 dcRecO (PDB ID: 1W3S). Displayed OB folds are colored ranging from blue at the N-terminus to red at the C-terminus. Displayed residues are assumed to interact with ssDNA. Residues thought to be important for ssDNA binding are shown in stick form. ssDNA is shown as lines.

3.0 Å. Good structural similarity was observed among the proteins despite no significant sequence similarity. In the Pfam classification of protein structures, the top structures found in the DALI search can be considered to have a five-stranded β-sheet coiled to form a closed β-barrel. This architecture is common to the OB-fold clan (Murzin, 1993), which contains 24 families in Pfam. For example, SSB is also a member of OB-fold domains. The DALI search with the ttRecJ-OB domain revealed significant matches (Z-score ~8 and r.m.s.d. <3.0 Å) with several SSBs from various species and PriB, a primasomal DNA replication protein of *E. coli*. Both SSB and PriB belong to the single-stranded binding protein family (PF00436) in Pfam. PriB can bind to not only ssDNA but also ssRNA (Liu *et al*., 2004; Lopper *et al*., 2004; Shioi *et al*., 2005; Huang *et al*., 2006). However, a BLAST search did not identify the region with any similarity to SSBs and PriB. Considering the low sequence similarity of RecJ-OB domains to the domains belonging to the OB-fold clan, I have proposed that the RecJ-OB domain is a novel member of the OB-fold superfamily. It should be noted that in the common architecture of the OB-fold, the β-sheet is capped by an α-helix located between the third and fourth strands in the majority of cases (Murzin, 1993); however, the ttRecJ-OB domain lacks such a helix. An OB-fold member that lacks such a helix is also included in the N-terminal of RecO from *Deinococcus radiodurans* (dcRecO) that is involved in homologous recombination (Makharashvili *et al*., 2004: Leiros *et al*., 2005). Nevertheless, this finding raised the possibility that the ttRecJ-OB domain is involved in binding to ssDNA. Experimental verification of this possibility will be described in a later section. The DALI search with residues 533–658 of ttRecJ did not identify structures having a Z-score above 4 and an r.m.s.d. below 3.0 Å. Sequence similarity was also low. These findings suggested that the

novel nature of this fold.

***Metal ion-binding sites*:** Electron densities corresponding to Mg^{2+} and Mn^{2+} ions were identified near the motifs I–IV in the hole between the domains I′ and II′. In the Mg^{2+} complex, I found the electron density for a single Mg^{2+} ion (Fig. 11B). The Mg^{2+} ion is coordinated in a near-perfect octahedral geometry by four oxygen atoms and two nitrogen atoms (Fig. 11B). The Mg^{2+} ion is coordinated with the side chain of Asp84 (2.31 Å, motif I), Asp136 (2.57 Å, motif II), His160 (2.55 Å, motif III), His161 (2.52 Å, motif III), Asp221 (2.37 Å, motif IV), and one water molecule (2.34 Å, W1).

On the other hand, in the Mn^{2+} complex, I found the electron densities for two Mn^{2+} ions (Mn1 and Mn2) using an anomalous difference Fourier map. While Mn1 is coordinated by four oxygen atoms and one nitrogen atom, Mn2 is coordinated by five oxygen atoms (Fig. 11C). Mn1 is situated at the same position as Mn^{2+} in cd-ttRecJ (Fig. 9) and Mg1. The density of Mn2 was much weaker than that of Mn1, and the B-factor of Mn2 (60) was higher than that of Mn1 (30). These results suggested that Mn2 had a lower occupancy than Mn1. Mn1 was coordinated to the side chain of Asp84 (2.38 Å, motif I), Asp136 (2.09 Å, motif II), His160 (2.27 Å, motifIII), Asp221 (2.04 Å, motif IV), and one water molecule (2.52 Å, W1). Mn2 was coordinated with the side chains of Asp80 (2.25 Å, motif I), Asp82 (2.30 Å and 2.54 Å, motif I), Asp136 (1.92 Å, motif II), and the same water molecule (2.54 Å, W1). The water molecule (W1) coordinated by the metal ions is located at the same position as in the ligand-free form (Fig. 11A).

***DNA-binding ability of the RecJ-OB domain*:** To investigate whether the OB-fold

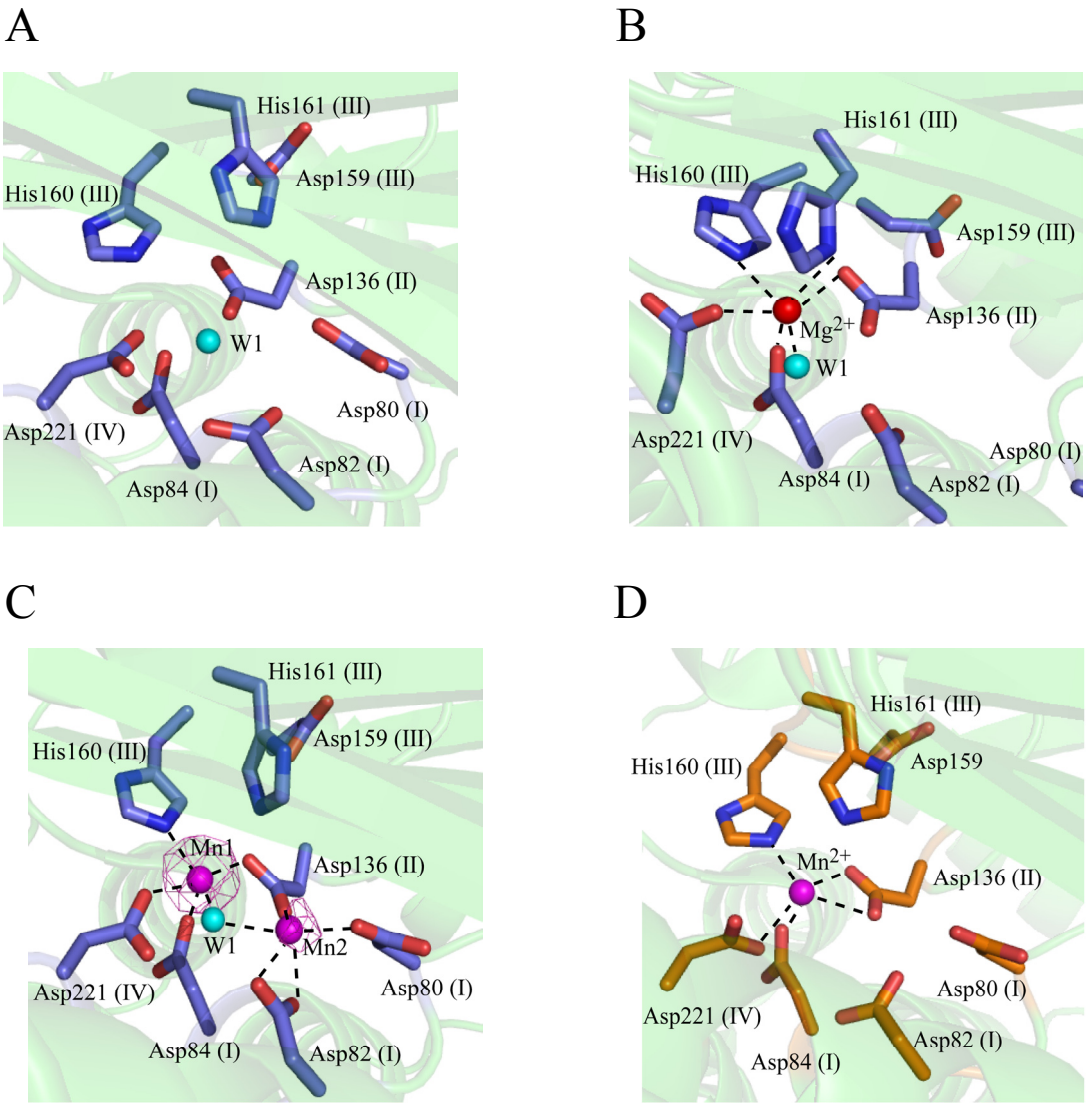

FIGURE 11. Metal ion-binding site. *A*, Intact ttRecJ apo form. *B*, Mg^{2+} ion-binding site in intact ttRecJ. The position of the Mg^{2+} ion is shown by a magenta ball. *C*, Mn^{2+} ion-binding sites in intact ttRecJ. The electron density (magenta) of the Mn^{2+} ions derived from the anomalous difference Fourier map (λ = 1.70000 Å) is superimposed on the model. The position of Mn^{2+} ion is shown by a magenta ball. *D*, Mn^{2+} ion-binding sites in cd-ttRecJ. The position of Mn^{2+} ion is shown by a magenta ball. W1, which is assumed to be the nucleophilic water, is shown by a cyan ball. Parentheses represent the name of the motifs. The dashed line shows the coordination with the metal ion.

domain (residues 457–532) binds to DNA or not, I prepared this domain (ttRecJ-OB domain) as a protein fragment. The His_6-tagged ttRecJ-OB domain was successfully overexpressed in *E. coli* and purified. It should be noted that the short stretch (GSHM) was added at the N-terminus after cleavage of the tag sequence.

The result of the gel shift assay showed that the intact RecJ could bind to ssDNA but not to dsDNA or ssRNA (Fig. 12A). The ttRecJ-ssDNA complex was found as a discrete band on the gel. This confirmed that RecJ is an ssDNA-specific exonuclease. In contrast, the ttRecJ-OB domain could bind to ssDNA and dsDNA but not to ssRNA (Fig. 12B). The protein-DNA complexes did not form a discrete band but smear bands on the gel. This suggested that the binding affinity of this domain to ssDNA was weaker than that of ttRecJ. This result supported the notion that the OB-fold domain of ttRecJ was involved in binding to ssDNA. It should be noted, however, that the ttRecJ-OB domain was able to bind to dsDNA, which was distinct from ttRecJ.

***Interaction of ttRecJ with ttSSB*:** To obtain further insight into the function of RecJ in DNA repair pathways, I investigated interaction of ttRecJ with ttSSB. The *ttssb* gene encodes a protein of 263 amino acids and has a calculated molecular mass of 29.9 kDa with a theoretical pI of 5.2. ttSSB was overexpressed in the soluble fraction in *E. coli* under the control of an IPTG-inducible T7 promoter. I purified the protein to homogeneity by using four-step column chromatography. The purified protein was identified to be ttSSB by MALDI-TOF MS with an overall MOWSE score of 216. Approximately 12 mg of ttSSB was obtained from 30 g of cells. This protein had an A_{280}/A_{260} ratio of 1.65, which suggested that the ttRecJ solution was not contaminated with any nucleotides. Size exclusion chromatography revealed that the apparent

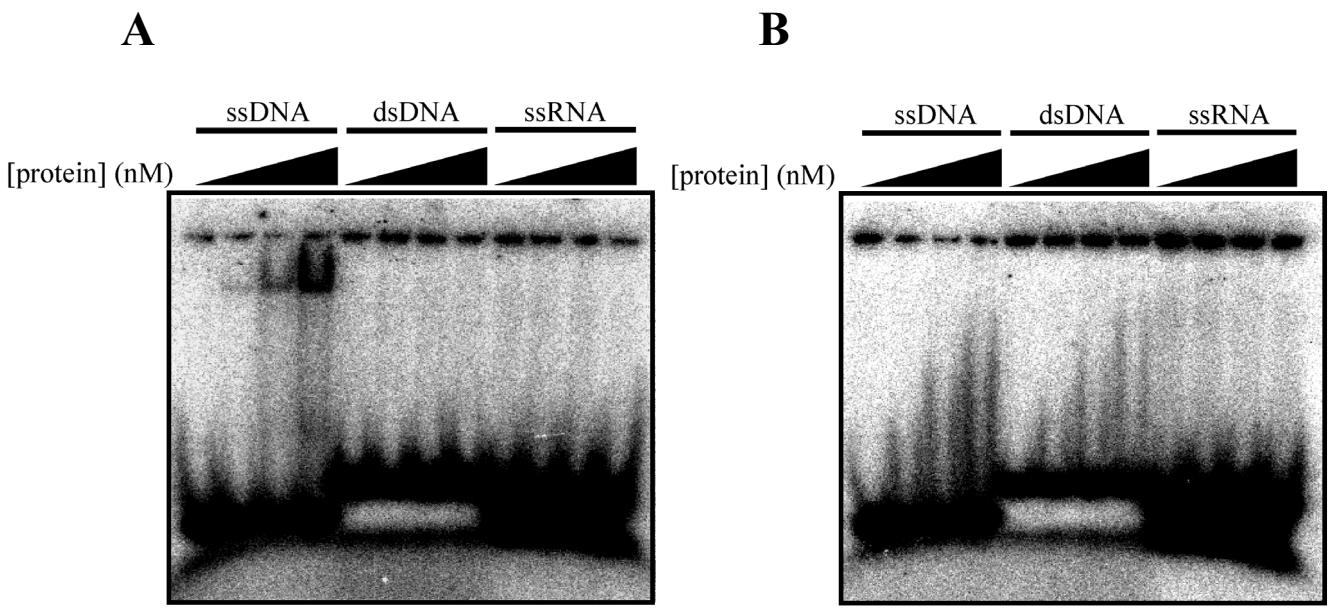

FIGURE 12. Gel shift assay with intact ttRecJ (A) and ttRecJ-OB domain (B). The reaction mixture, which contained 50 mM Tris-HCl, 100 mM KCl, 20 mM EDTA, 10 nM 5′-^{32}P-labeled 21-mer ssDNA (21f in Table 1) or 21-bp dsDNA (21f-21r in Table 1) or 21-mer ssRNA (21fR in Table 1), and 0, 100, 200, 400 nM protein (pH 7.5) was incubated at 37°C for 10 min.

molecular mass of ttSSB was 77 kDa (data not shown), which was approximately 2 time the calculated mass (29.9 kDa) from the sequence. This result indicated that ttSSB existed in a homodimer state in the solution along with other SSBs from *Deinococcus-Thermus* bacteria (Dabrowski *et al*., 2002; Dabrowski *et al*., 2002; Eggington *et al*., 2004).

I performed a gel shift assay to confirm whether ttRecJ interacted with ttSSB in the presence of 60-mer ssDNA (Fig. 13A). Upon the addition of ttRecJ alone, two shifted bands were observed, and the upper band was the major one. Because the length of the ssDNA used was relatively long, it was probable that two ttRecJ molecules bound to the 60-mer ssDNA, leading to the formation of the upper band. Moreover, upon the addition of ttSSB alone, two similar shifted bands were observed. When both ttRecJ and ttSSB were mixed with ssDNA, three bands were observed. Among them, the mobility of the lower two bands were identical to those of the ttSSB-ssDNA complexes. However, the top band was observed only in the presence of ttRecJ and ttSSB. Concomitantly, the band of the ttRecJ-ssDNA complex disappeared in these samples. These results suggested that the top band corresponded to a ttRecJ-ttSSB-ssDNA tertiary complex. Further, it was suggested that the affinity of ttSSB to ssDNA was stronger than that of ttRecJ to ssDNA. In this measurement, ttSSB was added to 60-mer ssDNA prior to the addition of ttRecJ. Therefore, these results suggested that ttRecJ interacted with ttSSB on ssDNA.

To confirm the interaction between ttRecJ and ttSSB, I examined whether ttSSB affected ttRecJ exonuclease activity (Fig. 13B). In this assay, ttSSB was added to ssDNA substrate prior to the addition of ttRecJ in the presence of 5 mM $MgCl_2$. Under these conditions, exonuclease activity was observed in the presence of ttRecJ

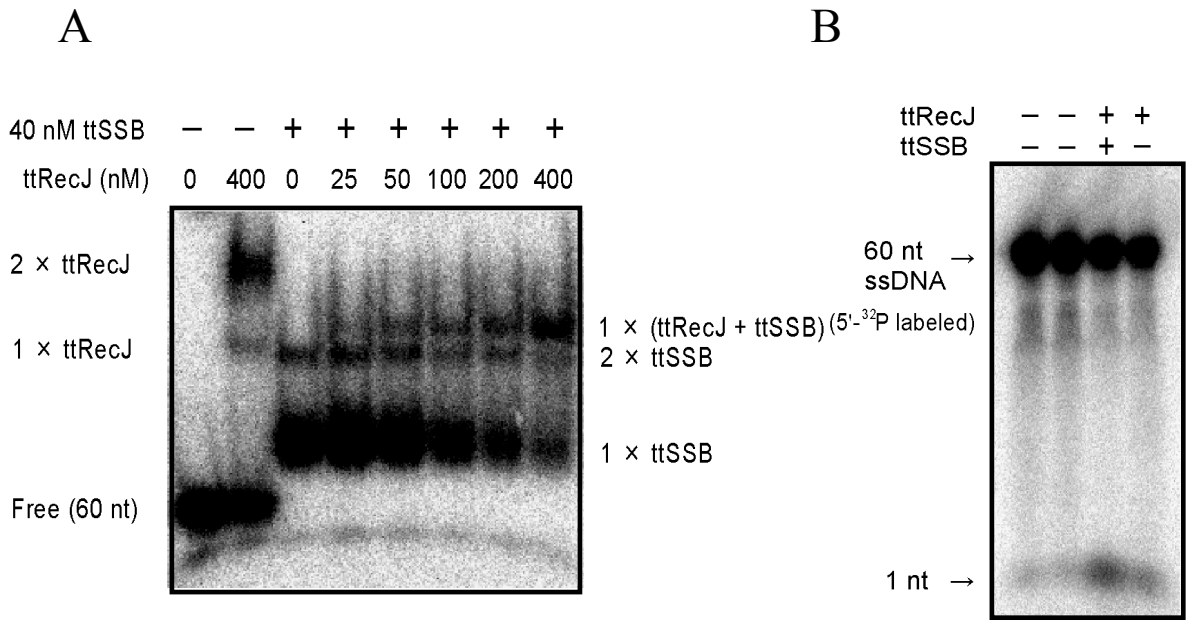

FIGURE 13. The interaction between ttRecJ and ttSSB in the presence of ssDNA. *A*, Gel shift assay. The reaction mixture, which contained 50 mM Tris-HCl, 100 mM KCl, 20 mM EDTA, 10 nM 5′-^{32}P-labeled 60-mer ssDNA, 40 nM (80 nM per monomer) ttSSB, and 0–400 nM ttRecJ (pH 7.5) was incubated at 37°C. ttSSB was allowed to bind to ssDNA for 10 min at 37°C prior to ttRecJ addition. *B*, Exonuclease activity. The reaction mixture, which contained 50 mM HEPES, 100 mM KCl, 5 mM $MgCl_2$, 10 nM 5′-^{32}P-labeled 60-mer ssDNA, 40 nM (80 nM per monomer) ttSSB, and 0.5 nM ttRecJ (pH 7.5) was incubated at 37°C for 20 min. ttSSB was allowed to bind to ssDNA for 10 min prior to ttRecJ addition.

alone. The addition of ttSSB stimulated the exonuclease activity of ttRecJ by approximately 2-fold. This result supported the notion that ttRecJ interacts with ttSSB in the presence of ssDNA.

Next, whether ttRecJ forms a complex with ttSSB in the absence of ssDNA was examined by ITC analysis (Fig. 14). In this binding assay, ttSSB was titrated with ttRecJ. The two-independent site-binding model with different affinities provided the best fit to the experimental data (Fig. 14, bottom panel). The N1 and N2 values were 1.35 and 1.90, respectively. The K_d1 and K_d2 values were 3.12 μM and 386 μM, respectively. The heat changes ($\Delta H1$ and $\Delta H2$) were –5.86 and –6.44 kcal/mol, the entropy changes ($\Delta S1$ and $\Delta S2$) were 10.1 and –0.615 cal/mol/deg, and the free energy change ($\Delta G1$ and $\Delta G2$) were –6.11 and –6.43 kcal/mol, respectively.

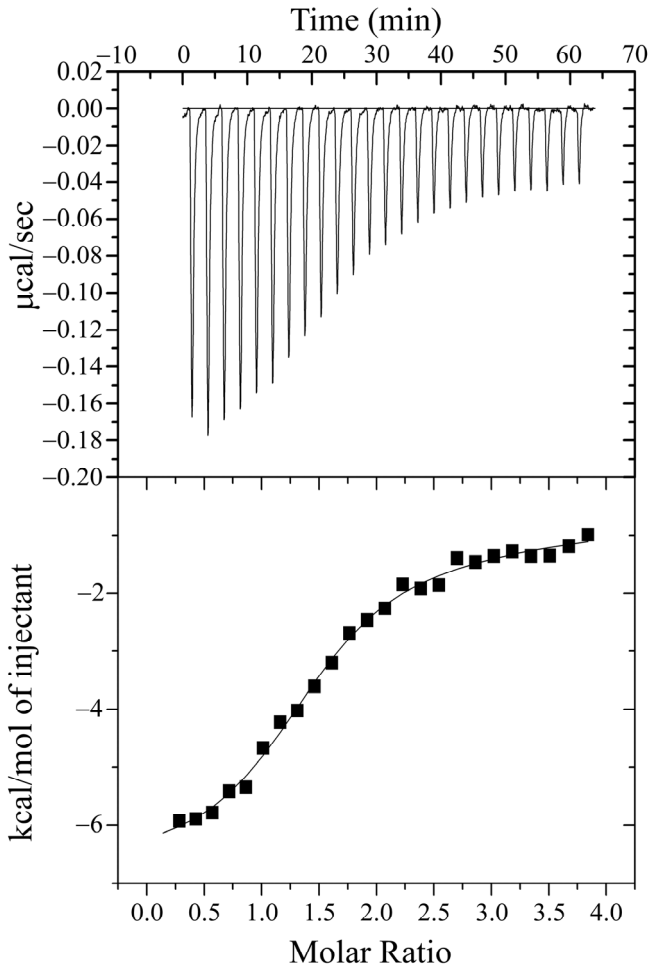

FIGURE 14. ITC experiments of ttRecJ-ttSSB interaction in the absence of ssDNA. *Top panel*, heat of interaction evolved by ttRecJ into a solution of ttSSB as described under "Experimental procedures". *Bottom panel*, binding isotherms corresponding to the data from the *top panel*. The line is the calculated curve from the two-independent site-binding model.

Discussion

In this study, I succeeded in determining the crystal structure of the intact ttRecJ. This is the first report of the three-dimensional structure of the intact RecJ protein. Our group previously determined the crystal structure of cd-ttRecJ, which lacks the N- and C-terminal regions of the intact protein (Yamagata *et al*., 2002). The structure of cd-ttRecJ is composed of two domains, which forms a groove containing the active site. In the intact structure, the arrangement of these two domains (domain II′ and III′) are almost the same as that in the cd-ttRecJ structure; however, the domain I′, consisting of the N- and C-terminal regions, is situated over the groove in the intact structure. Yamagata *et al*. have proposed a DNA-binding model based on the cd-ttRecJ structure, in which ssDNA simply binds to the groove (2002). However, the fact that the domain I′ is located over the groove and the active site is located within the hole and not in the groove needs to be considered for any further study. In the common core structures of T5 5′ exonuclease, FEN-I, and the N-terminal domain of *Taq* polymerase I, the active site is also located in a hole into which DNA is threaded (Ceska *et al*., 1996; Hosfield *et al*., 1998; Kim *et al*., 1995). However, these are structure-specific endonucleases and can bind to dsDNA with branched structures. Since RecJ exhibits no structure-specific nuclease activity, the DNA-binding mode and the mechanism of action of RecJ should be speculated upon based on the results of this study together with previous experimental data.

***Binding to DNA*:** The most important finding in this study is the presence of the OB-fold domain in domain I′. The OB-fold can be found in many DNA-binding

proteins (Theobald *et al*., 2003). I have shown here that the protein fragment consisting of this domain (residues 457–532) could bind to ssDNA and dsDNA but not to ssRNA. This result raises the possibility that the ttRecJ-OB domain is involved in binding to ssDNA. Structural and mutational studies of other OB-fold proteins revealed that binding to ssDNA is mediated by the following three major structural elements: the β1–β2 loop, the C-terminal part of β3, and the β4–β5 loop. The first region provides positively charged residues to form hydrogen bonds with the phosphate groups of the substrate, and the latter two provide one conserved aromatic side-chain to stack with the bases (Bochkarev and Bochkareva, 2004). In the ttRecJ structure, the residues in these three regions might be Arg472, Trp492, and Trp514, respectively (Figs. 5 and 10). These findings also support the notion that the ttRecJ-OB domain is involved in binding to ssDNA. However, Trp492 and Trp514 are not conserved in the RecJ protein according to the primary sequence information while Arg472 is conserved (Fig. 5). OB-folds also exist in RNA-binding proteins such like cold-shock proteins (Theobald *et al*., 2003); however, neither the ttRecJ-OB domain nor the intact ttRecJ could bind to ssRNA (Fig. 12B). The specificity of the ttRecJ-OB domain to ssDNA is probably ascribed to its structural features that are specific for ssDNA-binding subgroups of OB-fold proteins.

It can be supposed that ssDNA enters into the active site within the hole from the side where the OB-fold is located because the hole is more open on this side than the other non-OB-fold side (Fig. 8). Furthermore, highly conserved residues in domain I′ and II′, Arg110 (disordered in intact ttRecJ structure), Asn273, Arg277, Asn307, Arg310, Gln311, Arg350, and Arg370 (Fig. 5), whose side chains can interact with the backbone of the nucleic acid (in fact, it was proposed that Asn273, Arg277, and Arg370 were

responsible for the binding to ssDNA (Rajman and Lovett, 2000; Sutera *et al*, 1999), are located adjacent to the OB-fold (Fig. 15). If this is the case, the ttRecJ-OB domain can be considered to be situated at the entrance to the active site. Although a fragment of this domain could bind to dsDNA, the intact ttRecJ did not (Fig. 12). The size of the hole containing the active site is too narrow to bind to dsDNA. These results suggest that a stable complex of ttRecJ with dsDNA cannot be formed even if the ttRecJ-OB domain binds to dsDNA or dsDNA region in branched DNA forms. In addition, the affinity of this domain to ssDNA is weaker than that of the intact protein (Fig. 12) and the cd-ttRecJ lacking this domain exhibited 5′-3′ exonuclease activity comparable to the intact protein (Yamagata *et al*., 2001). Therefore, this domain might play a role in stabilizing the substrate complex by enhancing binding to ssDNA. The K_m for exonuclease activity of the intact ttRecJ (0.037 μM) was much lower than that of cd-ttRecJ (6.1 μM, Yamagata *et al*., 2001); the presence of the OB-fold domain is thought to be a reason for this difference (and the other reason will be discussed later). The C-terminal regions of all RecJ homologs display region similarity to the OB-fold domain, which supports the validity of the functional importance of this domain. The functional role of the OB-fold domain will also be discussed partly in chapter II.

In contrast to the OB-fold domain, the DALI search revealed a novel fold for residues 533–658 of ttRecJ. The C-terminal regions following this domain have diverse lengths and relatively low similarity among specificities (Figs. 3B and 5). Structurally, part of the C-terminal region interacts with the N-terminal region, which enables the formation of domain I′. However, the functional structure of the C-terminal region remains to be elucidated.

Since RecJ is a 5′-3′ exonuclease, it is obvious that RecJ can bind to 5′-end of

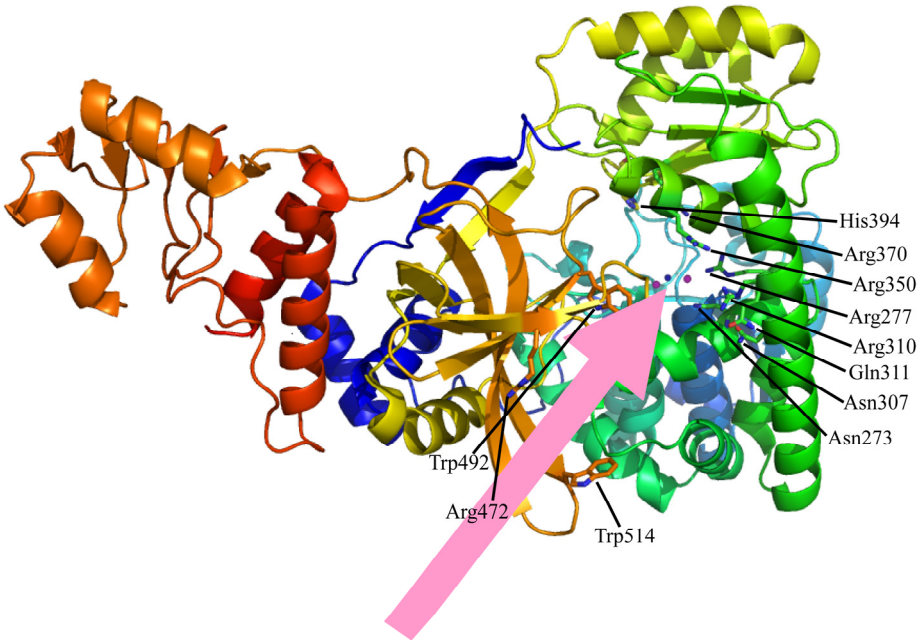

FIGURE 15. Model of ssDNA bound to ttRecJ. ssDNA is shown by a pink arrow. Side chains of the possible residues for ssDNA binding are shown as stick forms. A magenta ball and a blue ball (Mn^{2+} and W1, respectively, Fig. 11C) are shown.

ssDNA. However, the gel shift assay showed that two ttRecJ molecules could bind to 60-mer ssDNA. This raises the possibility that ttRecJ can bind to ssDNA even at the 3′-end and/or the non-terminal region. This notion may be supported by the observation that ttRecJ could bind to 29-mer 3′-overhang dsDNA (data not shown). In this experiment, the 3′-end of the overhang (ssDNA) region was an OH^- group. It was reported that the 5′-terminal phosphate group was not required for the binding and hydrolase activities of ecRecJ for ssDNA (Han *et al*., 2006). Thus, RecJ may bind at the 3′-end of ssDNA, but such interaction would result in the formation of a nonproductive complex. For the binding of ttRecJ at the non-terminal region, it must be assumed that ssDNA is threaded into the hole containing the active site. It is uncertain at present whether such a complex can be formed.

***Active site*:** Another important finding is the conformational change in the catalytic core domain. Yamagata *et al.* determined the cd-ttRecJ structure in complex with one Mn^{2+} ion, while I determined the intact ttRecJ structure in an apo form and in complex with two Mn^{2+} ions and with one Mg^{2+} ion (2002). Comparing the core domains between the cd-ttRecJ and intact forms, the movement of the loop containing the DHHA1 motif can be observed: this loop is placed closer toward the catalytic residues in the intact ttRecJ than in cd-ttRecJ (Fig. 9). This might be induced by interaction between the N- and C-terminal regions (domain III′) outside of the core domain. The distance between His-394 in the DHHA1 motif and the metal ion (Mg^{2+} or Mn1) in the intact ttRecJ (10 Å) was shorter than that (Mg^{2+}) in cd-ttRecJ (14 Å) (Fig. 9). Sutera *et al.* showed that the ecRecJ H429A mutant markedly decreased activity, suggesting the functional importance of this residue (1999). I hypothesize that this highly conserved

His residue is involved in the proper binding of ssDNA. The difference of the loop containing this His residue may be another reason for the differences in the K_m values.

Structural comparison also revealed the difference in the coordination state of the metal center. It is reported that the coordination number of Mg^{2+} and Mn^{2+} ions is usually six (Glusker, 1991). In the cd-ttRecJ structure (PDB ID: 1IR6), one Mn^{2+} ion was coordinated by the side chains of four amino acids (Asp84 (2.39 Å, motif I), Asp136 (2.63 Å and 2.64 Å, motif II), His160 (2.24 Å, motif III), and Asp221 (2.50 Å, motif IV)) with the other two sites being vacant (Yamagata *et al*., 2002). In the ttRecJ-Mg^{2+} complex, the Mg^{2+} ion was located at the same position as the Mn^{2+} ion in the cd-ttRecJ and coordinated by the side chains of five conserved residues (Asp84, Asp136, His160, His161, and Asp221) and a water molecule (W1). This coordination is identical as that in the cd-ttRecJ-Mn^{2+} complex except for the presence of W1 and His161. His161 is also located near the Mn^{2+} ion but too far for coordination (3.22 Å) in the cd-ttRecJ structure. This difference in the coordination appears to be owing to the conformational change. In the ttRecJ-Mn^{2+} structure, however, two Mn^{2+} ions are found in the active site and coordinated by pentahedral geometry. The Mn1 ion, located at the same position as the Mg^{2+} ion, is coordinated by Asp84, Asp136, His160, Asp221, and additionally, one water molecule (W1). The Mn2 ion is coordinated by Asp80, Asp82, Asp136, and W1. The side chain of Asp136 is situated at a position that can bridge the two Mn^{2+} ions. Asp80 and Asp82 are also included in motif I of additionally DHH superfamily. Of great importance for the catalytic mechanism, the same water molecule is coordinated by the two Mn^{2+} ions. In the *Saccharomyces cerevisiae* cytosolic exopolyphosphatase in another RecJ-like protein (RecJ-like family II), two metal cations are also coordinated by such a geometry in their active sites

(Ugochukwu *et al*., 2007; Tammenkoski *et al*., 2007). Therefore, I conclude that ttRecJ possessing two metal ions is an active form. ttRecJ exhibited similar metal ion requirements with hiRecJ (Sharma and Rao, 2009) and *S. cerevisiae* cytosolic exopolyphosphatase (Andreeva *et al*., 1998). In contrast, ecRecJ requires only Mg^{2+} for activity, while Mn^{2+} inhibited its activity (Lovvett *et al*., 1989). This distinct metal ion requirement suggested that the modes of metal ion binding of ttRecJ and hiRecJ differ from that of ecRecJ.

The water molecule (W1) near the two Mn^{2+} ions is a probable candidate for a nucleophile initiating an attack on the scissile phosphodiester bond of ssDNA because W1 is located in a site with access to ssDNA. Such coordination is consistent with a two-metal-ion mechanism of DNA cleavage as previously suggested for other nucleases (Beese and Steitz, 1991; Hosfield *et al*., 1998; Kovall and Matthews, 1999; Suck and Oefner, 1986; Mol *et al*., 1995; Nowotny *et al*., 2005; Perry *et al*., 2006). In the determined structures, no amino acid residue is liganded to W1, suggesting that this water molecule is activated by the metal ions. In other nucleases, metal ions are known to act as ligands to oxygen atoms of DNA phosphate groups. Although it is unknown at present how ttRecJ binds to ssDNA, Mn1 might be located to the 3′ side of the cleavage site and Mn2 to the 5′ side. Mn2 might interact with the 5′-terminal nucleotide of the substrate and also with the mononucleotide, a product generated by cleavage of the phosphodiester bond. The determined structures did not contain the second Mg^{2+} ion. Even in the Mn-complex, the affinity of Mn2 was thought to be weaker than that of Mn1. The binding of a nucleotide or ssDNA may stabilize the second metal ion, similar to *E. coli* DNA polymerase I (Beese and Steitz, 1991).

Mutational analysis of ecRecJ using crude extracts showed that substitution of Ala

for the conserved residues within motifs I–IV resulted in at least a 100-fold decrease in the exonuclease activity (Sutera *et al*., 1999), in which the target residues are: Asp79 (corresponding to Asp80 in ttRecJ; motif I), Asp81 (Asp82; motif I), Asp83 (Asp84; motif I), Asp137 (Asp136; motif II), Asp160 (Asp159; motif III), His161 (His160; motif III), His162 (His161; motif III), Asp236 (Asp221; motif IV), and His429 (His394; motif V). Among them, the necessity of Asp80, Asp82, Asp84, Asp136, His160, His161, and Asp 221 for the activity was verified by this study. Asp159 is located near the metal center and thus may fix the active site pocket via interaction with other residues. His394 faces the hole and may be involved in the proper binding of ssDNA as discussed previously. Outside the motifs, substitution of Arg401 (Arg370) also lost the activity (Sutera *et al*., 1999). Since Asp370 in domain III′ faces the hole but is far from the active site, it is probable that this residue is responsible for binding to ssDNA.

***Interaction with SSB*:** In homologous recombination and MMR, SSB acts to prevent reannealing and forming the secondary structure of ssDNAs behind the helicase; it was therefore proposed that RecJ acts on ssDNA bound to SSB. The ecSSB was reported to enhance the DNA binding and nuclease activity of ecRecJ, suggesting an interaction between these proteins (Han *et al*., 2006). Recently, hiSSB was reported to enhance the nuclease activity and interact with MBP-hiRecJ directly by using surface plasmon resonance analysis (Sharma and Rao, 2009). In this study, I successfully purified ttRecJ and ttSSB, both of which are intact proteins. Further, I found that the full-length residue of ttRecJ is longer than that of ecRecJ and hiRecJ (Figs. 3B and 5). ttSSB enhanced the ttRecJ nuclease activity (Fig. 13B); Sharma and Rao showed that this enhancement of activity was due to the inhibition of forming a

strong secondary structure of ssDNA, which interfered with RecJ nuclease activity and the decrease in the K_m value but not the increase in the k_{cat} value. While the K_m for MBP-hiRecJ was 10.9 μM in the absence of hiSSB and 3.3 μM in the presence of hiSSB, the k_{cat} (~0.74 s^{-1}) remained unchanged in the both cases. Thus, Sharma and Rao suggested that the affinity of RecJ for ssDNA was enhanced in the presence of SSB indicating that SSB could function in recruiting RecJ to ssDNA termini (2009). In this study, I also showed that ttSSB could directly bind to ttRecJ by using ITC analysis. The K_{d1} (3.1 μM) of the ttSSB-ttRecJ binding reaction was slightly greater than K_d (1.6 μM) of MBP-hiRecJ hiSSB (Sharma and Rao, 2009). The K_{d1} (3.1 μM) of the ttSSB-ttRecJ binding reaction was lesser than the K_d (6.4 μM) of ecSSB-*E.coli* RecQ (Shereda *et al*., 2007) and greater than that of ecSSB-*E. coli* ExoI (0.14 μM) (Lu and Keck, 2008). ttSSB enhanced ttRecJ exonuclease activity 2-fold, while ecSSB enhanced *E. coli* RecQ helicase activity (Shereda *et al*., 2007) and *E. coli* ExoI exonuclease activity 5- and 4-fold, respectively (Lu and Keck, 2008). In all cases examined to date, SSB-binding proteins are known to bind with the flexible C-terminal stretch (SSB-Ct), which consists of nine residues containing hydrophobic and acidic residues. MBP-hiRecJ failed to coprecipitate with hiSSB which lacked the last 41 residues from the C-terminal upon addition of ammonium sulfate. This indicated that the C-terminus of SSB mediated its interaction with RecJ (Sharma and Rao, 2009). In the case of ttSSB, the sequence of SSB-Ct is FPPEEELPF. In EcExoI and EcRecQ structures presumably, the C-terminal element of ecSSB binds to a hydrophobic pocket, in which a basic residue is positioned at the lip for recognition of the C-terminal Phe of SSB-Ct, while flanking basic residues bind to the conserved acidic residues of SSB-Ct (Lu and Keck, 2008; Shereda *et al*., 2009). Sharma and Rao suggested that hiSSB

interacted with hiSSB within the residues 35–498 (40–465 in ttRecJ) (2009). I attempted to identify the SSB-Ct-binding site in ttRecJ structure by analyzing the electrostatic potential map but could not identify any such candidate site. Thus, other methods (NMR, site-directed mutagenesis, etc.) will be required for identifying the binding site.

In conclusion, I have determined the three-dimensional structure of intact RecJ for the first time. These results may be useful in understanding the DNA repair and recombination systems in bacteria and archaea.

Chapter II

Functional analysis of a RecJ-like family I protein TTHA0118 from *Thermus thermophilus* HB8 and Mpn140 from *Mycoplasma pneumoniae*

Abstract

Exopolyphosphate-related proteins belonging to the RecJ-like family I have been proposed to be a candidate for oligoribonuclease and 3′-phosphoadenosine 5′-phosphate (pAp) phosphatase in bacteria and archaea, which do not have Orn (oligoribonuclease) and CysQ (pAp phosphatase) homologs. However, detailed analyses such as kinetic studies have not been reported. Here, we analyzed the biochemical and physiological characterization of TTHA0118 from *Thermus thermophilus* HB8 and Mpn140 from *Mycoplasma pneumoniae*. TTHA0118 and Mpn140 had high activity as ssDNA- and ssRNA-specific 5′-3′ exonuclease and pAp phosphatase. They hydrolyzed preferentially shorter ssDNA and ssRNA, whereas ttRecJ showed no such dependence on substrate length. Disruption of *ttha0118* gene led to growth retardation in minimal essential medium compared with wild *T. thermophilus* HB8. DNA microarray analysis showed that the disruptant Δ*ttha0118* suffered from several stresses in the minimal essential medium. Addition of mononucleotides (AMP, UMP, GMP, and CMP mixtures), nucleosides (adenosine, guanosine, cytidine, and uridine mixtures), or cysteine to the minimal essential medium increased the growth rate of the Δ*ttha0118* strain compared with that in the absence of these compounds. *Mycoplasmas* do not have the ability to synthesize nucleic acid precursors *de novo*; thus, this nuclease activity might be important in the production of precursors for the synthesis of nucleic acids. These results suggested that these exopolyphosphate-related proteins act in recycling shorter nucleotides to mononucleotides and controlling pAp concentrations *in vivo*.

Introduction

It is known that there are mainly two RecJ-like family I proteins other than RecJ proteins (N_155469), exopolyphosphatase-related proteins (family N_142143 in bacteria, family O_155470 in archaea), and putative poly(A) polymerase (family O_142140) according to the SYSTERS database (Krause *et al*., 1999). The three RecJ-like family I proteins in *T. thermophilus* HB8 are TTHA0118 (exopolyphosphatase-related proteins), TTHA0831 (putative poly(A) polymerase), and TTHA1167 (ttRecJ) (Fig. 3A). While TTHA0118 and ttRecJ have only DHH and DHHA1 pfam domains, TTHA0831 has another pfam domain (e.g., PolyA_pol pfam domain is a poly(A) polymerase head domain) in addition to these two. *T. thermophilus* HB8 has no RecJ-like family II protein, which instead has motifs I–IV and DHHA2 (Aravind and Koonin, 1998). ORFs-encoding exopolyphosphatase-related proteins are found in many bacterial genomes. However, study of these proteins has been quite primitive as compared to that of RecJ.

Recently, it was reported that the exopolyphosphatase-related protein YtqI from *Bacillus subtilis* hydrolyzed short-length ssRNA and 3′-phosphoadenosine 5′-phosphate (pAp) in the presence of $MnCl_2$ *in vitro* and was able to complement both *orn* (oligoribonuclease) and *cysQ* (pAp phosphatase) mutants in *E. coli*. *E. coli* Orn and its human homolog Sfn (small fragment nuclease) degraded both ssDNA and ssRNA with a length of 5 mer or shorter to mononucleotides in a 3′–5′ direction. This exonuclease activity had a strong dependence on the Mn^{2+} ion (Nguyen *et al*., 2000). The *orn* mutant of *E. coli* showed the accumulation of short ssRNA (Ghosh and Deutscher, 1999). The mRNA-degrading exonucleases, such as RNase II and polynucleotide phosphorylase,

cannot degrade ssRNA (oligoribonucleotide) shorter than 10-mer (Niyogi and Datta, 1975; Datta and Niyogi, 1975). In contrast, the turnover number of YtqI for 3-mer ssRNA was approximately 10-fold greater than that for 5-mer ssRNA (Mechold *et al*., 2006). These observations suggested that Orn-type oligo(deoxy)ribonucleases participate in mRNA degradation and cellular nucleotide recycling in these organisms (Datta and Niyogi, 1975; Zhang *et al*., 1998; Nguyen *et al*., 2000).

CysQ hydrolyzes pAp generated from phosphoadenosine 5′-phosphosulfate (PAPS) in the intermediate step of sulfate assimilation to 5′-AMP and Pi (Neuwald *et al*., 1992; Klaassen and Boles, 1997; Hatzios *et a*l., 2008). pAp is known to act as a competitive inhibitor of enzymes that use PAPS, i.e., mainly PAPS reductase and sulfotransferase that are involved in sulfate and cysteine assimilation (Klaassen and Boles, 1997) and nucleoside diphosphate kinase (Schneider *et al*., 1998) and Xrn1p that are involved in RNA hydrolysis (Dichtl *et al*., 1997). Because high pAp cell concentrations are toxic, controlling the pAp concentration is essential. Interestingly, Orn and CysQ are present in beta and gamma Proteobacteria and in Actinobacteria, whereas exopolyphosphatase-related proteins belonging to RecJ-like family I are absent in the majority of these bacteria. On the other hand, exopolyphosphatase-related proteins are present in Firmicutes, Bacteroidetes, Chlobi, and the delta subdivision of Proteobacteria, Crenachaeota, and Euryarchaeota, whereas Orn and CysQ are absent in the majority of these bacteria and archaea. This phylogenetic distribution suggests some anti-correlation (Mechold *et al*., 2007). However, biochemical properties of exopolyphosphatase-related proteins have not been investigated in detail. There is little detail regarding the polarity, cleavage pattern, kinetic constants, and metal ion dependence of the exonuclease and pAp phosphatase activities *in vitro*. In addition,

the detailed phenotype of the deletion mutant of exopolyphosphatase-related proteins has also been examined.

Recently, the crystal structure of the YtqI homolog BF3670 from *Bacteroides fragilis* has been resolved (Fig. 4. PDB ID: 3DMA) but has not been reported as an article. Exopolyphosphatase-related proteins are smaller in size than RecJ (Fig. 3A), although both contain the DHH motifs (I–IV) and DHHA1 motif (motif V). The overall structure of BF36780 is similar to that of cd-ttRecJ. The cleft containing motifs I–IV and DHHA1 is too narrow (13 Å wide) to accommodate DNA. At present, however, it seems difficult to exploit this structural information effectively for elucidating the structure-function relationship partly because its biochemical properties are little known. The structure alone is insufficient for infer the function *in vivo*.

In this study, I purified and performed the characterization of enzyme activity of TTHA0118 from *T. thermophilus* HB8. TTHA0118 had high k_{cat}/K_m parameters for oligo(deoxy)ribonuclease activity for short ssDNA and ssRNA as well as pAp phosphatase activity. Δ*ttha0118 T. thermophilus* HB8 led to growth retardation compared with the wild-type strain. DNA microarray data showed that the Δ*ttha0118* strain suffered from stress in the minimal essential medium. Moreover, the addition of 5′-mononucleotides, nucleosides, or cysteine to the minimal essential medium increased the growth rate of Δ*ttha0118*. These results suggested that TTHA0118 acts in recycling short oligonucleotides to mononucleotides and controlling the pAp concentration *in vivo*. Furthermore, I characterized the enzymatic properties of Mpn140, an exopolyphosphatase-related protein of *Mycoplasma pneumoniae* because *Mycoplasma* species have no enzyme for the *de novo* biosynthesis of nucleic acid precursors (Himmelreich *et al*., 1996; Pollack *et al*., 1997; Razin, 1978), and

Mycoplasma nucleases are thought to play a metabolic role in the production of nucleic acid precursors from the host (Minion *et al*., 1993; Bendjennat *et al*., 1997; Jarvill-Taylor *et al*., 1999; Schmidt *et al*., 2007).

Experimental procedures

***Materials*:** DNA-modifying enzymes, including restriction enzymes and LA Taq polymerase, were obtained from Takara Bio Inc. Yeast extract and polypeptone were from Difco. The DNA oligomers were synthesized by BEX Co. [γ-^{32}P]ATP was from ICN. All other reagents used were of the highest commercially available grade.

***Purification of TTHA0118*:** Using the *T. thermophilus* HB8 genome (DDBJ/EMBL/GeneBank AB107660) sequence information, I synthesized two primers for the amplification of the target gene (*ttha0118*) by PCR. Amplification was carried out according to standard protocols, and the amplified gene fragment was ligated into pT7Blue T-vector by TA cloning and confirmed by sequencing. The fragment bearing the target gene from pT7Blue-*ttha0118* was ligated into pET-11a at the *Nde*I and *Bam*HI sites. *E. coli* BL21(DE3) (TaKaRa) cells transformed with the resulting plasmid were cultured at 37°C to 4×10^8 cells/mL in 1.5 L of LB medium containing 50 μg/mL ampicillin. The cells were then incubated for 6 h in the presence of IPTG, harvested by centrifugation, and stored at –20°C.

All of the following procedures were carried out at room temperature unless stated otherwise. Frozen cells (10 g) were thawed, suspended in 100 mL of buffer I, and disrupted by sonication on ice. The lysate was incubated at 70°C for 15 min and centrifuged (38,000 *g*) for 60 min at 4°C. The resultant supernatant was loaded onto a Toyopearl SuperQ-650M column (bed volume, 20 mL) equilibrated with buffer II. Proteins were eluted with a linear gradient of 0–1 M NaCl (total volume, 250 mL). Ammonium sulfate was added to the fractions containing the TTHA0118 protein to a

final concentration of 1.5 M. The protein solution was then applied to a Toyopearl Ether-650S (Tosoh) column (bed volume, 20 mL) equilibrated with buffer II containing 1.5 M ammonium sulfate. The proteins were eluted with a linear gradient of 1.5–0 M ammonium sulfate (total volume, 250 mL). Fractions containing the TTHA0118 protein were collected and concentrated by a Vivaspin (cutoff MW, 30000) concentrator. The concentrated solution was applied to a Superdex 200 HR 10/30 column equilibrated with buffer III and eluted with the same buffer using an ÄKTA explorer system. The fractions containing the TTHA0118 protein were concentrated and stored at 4°C. At each step, the fractions were analyzed by SDS-PAGE. The concentration of the purified protein was determined by using the molar absorption coefficient at 278 nm calculated according to the formula of Kuramitsu *et al*. (1990).

***Purification of Mpn140*:** The *M. pneumoniae* M129 genome was provided by Dr. Naoto Ohtani (Keio University). The coding sequence for Mpn140 was amplified by PCR. To express it in *E. coli*, system site-directed mutagenesis was used to change the TGA codon, which encodes a tryptophan in *Mycoplasma*, to TGG. The PCR-amplified fragment was restricted with *Nde*I and *Bam*HI, and subcloned into the pET-11a expression vector. *E. coli* Rosetta(DE3) (Merck) cells transformed with the resulting plasmid were cultured at 37°C to 4×10^8 cells/mL in 1.5 L of LB medium containing 50 μg/mL ampicillin. The cells were then incubated for 6 h in the presence of IPTG, harvested by centrifugation, and stored at –20°C.

All of the following procedures were carried out at 4°C except for size exclusion chromatography. Frozen cells (15 g) were thawed, suspended in 150 mL of buffer I, and disrupted by sonication on ice. The lysate was centrifuged (38,000 *g*) for 60 min.

The resultant supernatant was loaded onto a Toyopearl SP-650M (Tosoh) column (bed volume, 20 mL) equilibrated with buffer II. Proteins were eluted with a linear gradient of 0–1 M NaCl (total volume, 200 mL). Ammonium sulfate was added to the fractions containing the Mpn140 protein to a final concentration of 1.5 M. The protein solution was then applied to a Toyopearl Ether-650S (Tosoh) column (bed volume, 15 mL) equilibrated with buffer II containing 1.5 M ammonium sulfate. The proteins were eluted with a linear gradient of 1.5–0 M ammonium sulfate (total volume, 150 mL). Fractions containing the Mpn140 protein were collected and concentrated by a Vivaspin (cutoff MW, 30000) concentrator. The concentrated solution was applied to a Superdex 200 HR 10/30 column equilibrated with buffer III and eluted with the same buffer using an ÄKTA explorer system. The fractions containing the Mpn140 protein were concentrated and stored.

***Spectroscopic analysis*:** Circular dichroism (CD) spectra in the far-UV region (200 nm to 250 nm) were obtained at 25°C with a Jasco spectropolarimeter, J-720W, using 5 μM of TTHA0118 or Mpn140 enzyme in 50 mM potassium phosphate and 100 mM KCl (pH 7.5). Thermostability was investigated by recording the molar ellipticity at 222 nm from 25°C to 95°C under the same conditions as above.

***Size exclusion chromatography*:** The enzyme (50 μM) was applied onto the Superdex 200 HR 10/30 column and eluted with buffer III with a flow rate of 0.5 mL/min by the ÄKTA system. The apparent molecular weight was estimated by comparing its retention time with those of molecular weight markers (Sigma).

***Assay for exonuclease activity*:** Oligo(deoxy)ribonucleotides used as the substrate are shown in Table 1. These ssDNAs or ssRNAs were radiolabeled at the 5′-end with [γ-^{32}P]ATP using polynucleotide kinase. The reaction mixture (10 μL), which contained 50 mM HEPES, 100 mM KCl, 5 mM $MnCl_2$, 10 nM 5′-^{32}P-labeled ssDNA, ssRNA or 5′-end 6-mer overhang dsDNA, various concentrations of cold ssDNA, ssRNA or 5′-end 6-mer overhang dsDNA, and various concentrations of TTHA0118 and Mpn140 (pH 7.5), was incubated at 37°C. For each time point, the reaction was quenched by the immediate addition of 1 μL of 100 mM EDTA and 11 μL of phenol/chloroform. The samples were centrifuged, and the equal volume of sample buffer (5 mM EDTA, 80% deionized formamide, 10 mM NaOH, 0.1% bromophenol blue and 0.1% xylene cyanol) was added to the supernatant. The samples were denatured at 95°C for 3 min, and were loaded onto a 25% (w/v) acrylamide gel containing 8 M urea and 1 × TBE buffer, and then electrophoresed in 1 × TBE buffer (Yamagata *et al*., 2001). The gel was dried and placed in contact with an imaging plate. The bands were visualized and analyzed using a BAS2500 image analyzer (Fuji Photo Film).

The percentage of degraded DNA or RNA was plotted for each incubation period. As the plot showed a linear region, the initial rate of the reaction could be obtained. The initial rate was plotted against the concentration of the substrate. The data were fitted to the Michaelis-Menten equation, and the kinetic constant was calculated by the software Igor Pro 3.14 (WaveMetrics).

To determine the products, the reaction mixture was applied to a reversed-phase column (CAPCELL PAK C18, Shiseido, 4.6 × 75 mm) equilibrated with 50 mM Tris-HCl (pH 8.0), 5 mM tetra-*n*-butylammonium phosphate, and 10% methanol. Elution was performed by a gradient of 10% to 50% methanol (Wakamatsu *et al*., 2008).

The reaction mixture (100 μL), which contained 50 mM HEPES, 100 mM KCl, 5 mM $MnCl_2$, 75 μM 6-mer ssDNA, and 0.5 μM TTHA0118, was incubated at 37°C for 60 min.

Exonuclease activity in the presence of various divalent cations was measured at 37°C using the following mixture: 50 mM HEEPES, 100 mM KCl, 5 mM divalent cation ($MgCl_2$, $MnCl_2$, $ZnCl_2$, $CoCl_2$, $NiCl_2$, or $CaCl_2$), 10 nM 5′-^{32}P-labeled ssDNA, 5 μM cold ssDNA, and 25 nM of enzyme.

***Assay for pAp phosphatase*:** To determine the steady-state kinetic parameters, the hydrolytic activities were analyzed by measuring the production of inorganic orthophosphate using a colorimetric assay (Wakamatsu *et al*., 2008). The reaction mixture (100 μL) which contained 50 mM Tris-HCl, 100 mM KCl, 5 mM $MnCl_2$ or $MgCl_2$, 0–1000 μM pAp, and 0.2 nM TTHA0118 or Mpn140, pH 7.5, was incubated at 37°C. To determine the products, the following reaction mixture was applied to CAPCELL PAK C18 column similar to the abovementioned method. The reaction mixture (100 μL), which contained 50 mM Tris-HCl, 100 mM KCl, 5 mM $MnCl_2$, 1 mM pAp, and 1 μM TTHA0118, was incubated at 37°C for 15 min.

***Assay for cAMP and cGMP phosphodiesterases*:** To determine the steady-state kinetic parameters, the following reaction mixture was applied to CAPCELL PAK C18 column similar to the abovementioned method. The reaction mixture (100 μL) which contained 50 mM Tris-HCl, 100 mM KCl, 5 mM $MnCl_2$, 0–2000 μM cAMP or cGMP, and 1 μM TTHA0118 (pH 7.5), was incubated at 37°C.

***Disruption of ttha0118 and growth analysis*:** Disruption of *ttha0118* (Δ*ttha0118*) *T. thermophilus* HB8 was constructed by homologous recombination using a thermostable kanamycin-resistant marker (Hashimoto *et al*., 2001). Wild and Δ*ttha0118* strains were grown at 70°C in a rich (TT) medium, TT plate, or minimal essential (CS) medium. TT medium contained the following components: 0.4% trypton, 0.2% yeast extract, 0.1% NaCl, 0.4 mM $MgCl_2$, and 0.4 mM $CaCl_2$ (pH 7.3, adjusted with NaOH). The TT plate contained 1.5% gelan gum in addition to the abovementioned components. CS medium contained the following components: 2% sucrose, 2% sodium glutamate, 0.055% K_2HPO_4, 0.018% KH_2PO_4, 0.2% NaCl, 0.05% $(NH_4)_2SO_4$, 0.0125% $MgCl_2$ $6H_2O$, 0.0025% $CaCl_2$ $2H_2O$, 0.001% $FeSO_4$ $7H_2O$, 0.00012% $NaMoO_3$ $2H_2O$, 0.00001% $VoSO_4$ xH_2O, 0.00005% $MnCl_2$ $4H_2O$, 0.000006% $ZnSO_4$ $7H_2O$, 0.0000015% $CuSO_4$ $5H_2O$, 0.00008% $CaCl_2$ $6H_2O$, 0.000002% $NiCl_2$ $2H_2O$, 0.001% biotin, and 0.01% thiamine (pH 7.3, adjusted with NaOH). Mononucleotide mixtures (AMP, GMP, CMP, and UMP mixtures), nucleoside mixtures (adenosine, guanosine, cytidine, and uridine mixtures), or cysteine were added to the CS medium (final concentration, 0.1 mM). Cultures used for growth studies with TT and CS media were initiated at approximately 4×10^4 cells/mL from preincubation TT cultures. Aliquots of the resulting cultures were taken 21 h previously, diluted appropriately, and counted using a cell counter. In TT plate cultivation, diluted bacterial cultures from preincubation TT cultures (3×10^7 cells/mL) were spread to 5×10^2 colonies/plate.

***DNA microarray*:** The cells of wild and Δ*tttha0118* strains were cultured in CS medium and harvested in the early log phase (cell density, 7×10^8 cells/mL). The treatments from the RNA isolation to the hybridization were performed as previously

described (Shinkai *et al*., 2007). For biological sample replication, both strains were grown four times independently, and the total RNA from each sample was evaluated using a DNA microarray system (Affymetrix GeneChip; Affymetrix Inc.). The probe array was scanned with a GeneArray scanner (Agilent Tech.) and the data analysis was performed by using GeneSpring GX (Agilent Tech.). The intensities for the Δ*ttha0118* strain samples were normalized by those for wild samples and used for the calculation. For the filtration, genes having the "Presence" flag in more than four samples were used for the analysis. Finally, genes with an average change of at least 2-fold and an initial *P* value of <0.05 for each replicate between wild and Δ*ttha0118* strains were considered to be significantly differentially expressed. The microarray data was deposited in the NCBI Gene Expression Omnibus (GEO; http://www.ncbi.nim.gov/geo/) and are accessible through the GEO Series accession number GSE12590.

Results

***Preparation of TTHA0118 and Mpn140*:** The *ttha0118* and *mpn140* genes encode proteins of 324 and 324 amino acids each with a calculated molecular mass of 35.1 and 37.2 kDa, and a theoretical pI of 5.2 and 9.2, respectively. These amino acid sequences contain motifs I–IV and the DHHA1 motif; however, the C-terminal regions of TTHA0118 and Mpn140 are shorter than those of RecJ proteins (Fig. 3). These three proteins were overexpressed in the soluble fraction in *E. coli* under the control of an IPTG-inducible T7 promoter. TTHA0118 was purified to homogeneity by using heat treatment and three-step column chromatography (Fig. 6A, lane 1). I also purified Mpn140 to homogeneity by using three-step column chromatography (Fig. 6A, lane 2). The purified proteins were identified to be TTHA0118 and Mpn140 by MALDI-TOF MS with an overall MOWSE score of 140 and 100, respectively. Approximately 3 mg of TTHA0118 and 2 mg of Mpn140 was obtained from 10 g and 15 g of cells, respectively.

***Physiochemical properties*:** Size exclusion chromatography was performed to investigate the oligomeric state of TTHA0118 and Mpn140. The apparent molecular mass corresponding to the peak was estimated to be 550 kDa and 58 kDa (Fig. 6B), which was approximately 15.6 and 1.5 times the mass (35.1 kDa and 37.2 kDa) calculated from the sequence, respectively. These results suggest that TTHA0118 exists in an oligomeric form; and Mpn140, in a monomeric or dimeric form in solution. Considering that cd-ttRecJ is a monomer (Yamagata *et al*., 2001) but BF3670 is probably a dimer, it was not turned out whether Mpn140 was monomer or dimer. The

far-UV (200–250 nm) CD spectra suggested that TTHA0118 and Mpn140 have a α/β or α +β fold (data not shown). TTHA0118 and Mpn140 were stable up to 85°C and 55°C at pH 7.5, respectively (data not shown).

***Enzymatic activity of TTHA0118*:** Exonuclease activity was analyzed with 5′-end-labeled ssDNA, ssRNA, and dsDNA with a 5′-overhang. The reaction of TTHA0118 with the labeled 11-mer ssDNA (11f in Table 1) in the presence of $MnCl_2$ gave only one radioactive band on the gel (lanes 3–4 in Fig. 7). This small-sized band corresponded to the labeled mononucleotide (1-nt), which was released from the 5′-end of the substrate. This result was similar to that of ttRecJ in the presence of $MgCl_2$ (lanes 7–8 in Fig. 7). Since RecJ is known to be a 5′-3′ exonuclease, these results suggested that TTHA0118 had 5′-3′ exonuclease activity for ssDNA. It should be mentioned that the position of 1-mer in lanes 3–4 was different from that in lanes 7–8. This was due to a difference in the species of the metal ion used (lanes 1 and 2 in Fig. 7). In the presence of $MnCl_2$ and $MgCl_2$, 1-mer was produced even without an enzyme, and the band positions of this product differed between these metal species.

The products of TTHA0118 5′-3′ exonuclease activity with 6-mer ssDNA was analyzed by HPLC (Fig. 16). Peaks eluted at 15.1, 8.8, 4.9, 2.2, 1.3, and 1.0 mL probably corresponded to 5- to 1-mer oligonucleotides. This result suggested that mononucleotides were formed as products of a TTHA0118-catalyzed reaction, possibly in a processive manner. Furthermore, because the 5′-end of the substrate 6-mer ssDNA was not phosphorylated, this data showed that TTHA0118 could degrade 6-mer ssDNA with either a 5′-OH or 5′-phosphate terminus. However, the k_{cat} value for

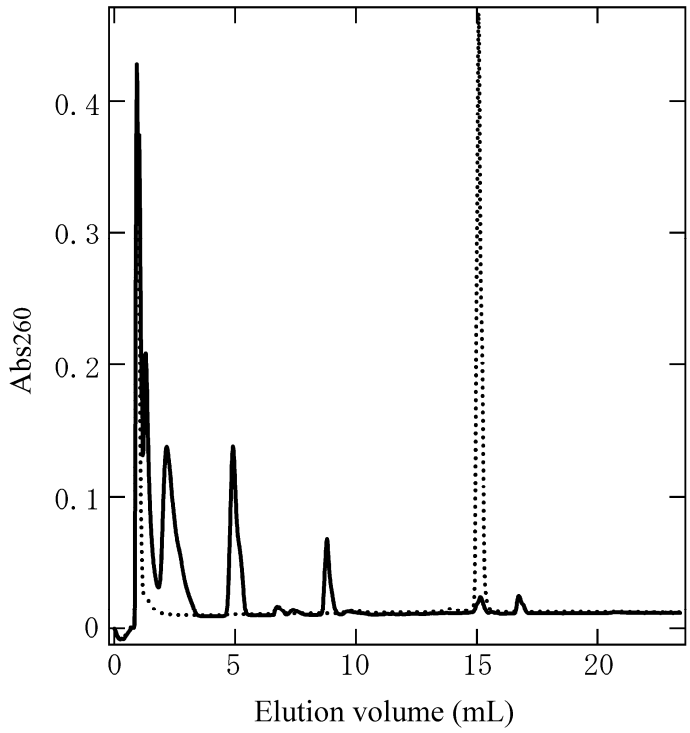

FIGURE 16. HPLC profile of the products in TTHA0118 exonuclease activity. Elution profile of the product of TTHA0118-catalyzed reaction with 6-mer ssDNA (6f in Table 1) (solid line) and a control mixture (dotted line). The enzyme reaction mixture was prepared as described under "Experimental procedures". Control mixture was prepared without TTHA0118.

6-mer ssDNA with a 5′-OH terminus was approximately 10% of that with a 5′-phosphate terminus. This differed from ecRecJ, which had exonuclease activity for both 5′-OH and 5′-phosphorylated substrate to a similar extent (Han *et al.*, 2006). TTHA0118 also hydrolyzed the ssDNA region of dsDNA with a 6-mer overhang at the 5′-end (33f-27r) and ssRNA (11fR) in the same degradation pattern as ssDNA, i.e., the 5′-labeled mononucleotide (1-mer) was released as a product (data not shown). These results indicated that TTHA0118 degraded ssDNA (or ssDNA region) and ssRNA in a 5′-3′ direction.

The presence of a divalent cation was essential for TTHA0118 exonuclease activity. Among the divalent cations examined (each at 5 mM) in 6-mer ssDNA degradation, Co^{2+} was the most effective cation and Mn^{2+} was second. The k_{app} values in the presence of Mn^{2+}, Zn^{2+}, Mg^{2+}, Ca^{2+}, and Ni^{2+} were approximately 51%, 16%, 15%, 11%, and 8%, respectively, of that in the presence of Co^{2+}. No activity was observed without a metal ion.

TTHA0118 hydrolyzed short ssDNA and ssRNA more efficiently than long ssDNA and ssRNA (Table 4). The k_{cat}/K_m values for 3-, 6-, 11-, and 21-mer ssDNA (Table 1) were 3.1×10^6, 3.3×10^4, 3.7×10^2, and 6.0×10 $M^{-1}s^{-1}$, respectively. Similarly, 3-, 6-, 11-, and 21-mer ssRNA (Table 1) showed 1.2×10^6, 2.3×10^4, 5.6×10^3, and 1.3×10^2 $M^{-1}s^{-1}$, respectively. The K_m values did not differ greatly among the examined oligonucleotides; the average values for ssDNA and ssRNA were 1.2×10^2 and 4.1×10^2 μM, respectively. However, the shorter the length of the substrate, the greater was the increase in the k_{cat} values; the values for ssDNA varied by approximately 5 orders of magnitude. No significant difference in the k_{cat} values were observed between ssDNAs and ssRNAs. Compared to ssDNA, degradation of the 5′-overhang dsDNA

TABLE 4. Kinetic constants for the exonuclease activity of TTHA0118 and Mpn140.

Assays were performed at pH 7.5 as described under "Experimental procedures".

Protein	Substrate	K_m (μM)[a]	k_{cat} (s^{-1})[a]	k_{cat}/K_m ($M^{-1}s^{-1}$)
TTHA0118	3f	6.5×10	2.0×10^{2}	3.1×10^{6}
	6f	2.8×10^{2}	9.1	3.3×10^{4}
	11f	6.8×10	2.5×10^{-2}	3.7×10^{2}
	21f	7.8×10	4.7×10^{-3}	6.0×10
	33f-27r	1.2×10^{2}	5.2×10^{-3}	4.3×10
	3fR	2.4×10^{2}	2.9×10^{2}	1.2×10^{6}
	6fR	2.7×10^{2}	6.2	2.3×10^{4}
	11fR	4.5×10^{2}	2.5	5.6×10^{3}
	21fR	6.8×10^{2}	8.8×10^{-2}	1.3×10^{2}
Mpn140	6f (Mg^{2+})	7.5×10^{-1}	4.5×10^{-1}	6.0×10^{5}
	6f (Mn^{2+})	1.5	1.2×10^{-2}	8.0×10^{3}
	11f (Mn^{2+})	3.5	2.8×10^{-3}	8.0×10^{2}
	6fR (Mg^{2+})	3.2×10^{-1}	3.3×10^{-2}	1.0×10^{5}
	6fR (Mn^{2+})	9.6×10^{-1}	1.0×10^{-2}	1.0×10^{4}
	11fR (Mn^{2+})	2.9	3.8×10^{-3}	1.3×10^{3}

[a] K_m and k_{cat} were determined from a nonlinear regression analysis.
The metal used is shown in parentheses.
33f-27r indicates that it is a 5′-end 6-mer overhang dsDNA. 33f was radiolabeled at the 5′-end with [γ-^{32}P]ATP.

(33f-27r) by TTHA0118 was much less efficient; the k_{cat}/K_m value for dsDNA with a 6-mer overhang was 1.3% of that for 6-mer ssDNA.

In contrast, ttRecJ in the presence of Mg^{2+} did not show any such dependence on substrate length (Table 4). It should be noted here that the kinetic constants of ttRecJ were determined in the presence of $MgCl_2$ because the presence of 5 mM $MnCl_2$ resulted in approximately 65% of the k_{app} for 21-mer ssDNA observed in the presence of $MgCl_2$. Affinity of ttRecJ to ssDNA was higher than that of TTHA0118. However, the K_m and k_{cat} values were similar for 6-, 11-, and 21-mer ssDNA, and the k_{cat}/K_m values for them were also almost the same. These results suggested that TTHA0118 and ttRecJ had a difference in substrate recognition although both belong to RecJ-like family I.

Furthermore, TTHA0118 exhibited phosphohydrolase activity for pAp (Table 5), similarly to *B. subtilis* YtqI. HPLC analysis revealed that the main peak eluted at 7.5 mL corresponded to 5′-AMP (Fig. 17), indicating that the reaction of TTHA0118 with pAp generated 5′-AMP, not 3′-AMP, as a product. Thus, the reaction formula of pAp phosphatase reaction was assumed to be follows: pAp + H_2O → 5′-AMP + inorganic phosphate. TTHA0118 had high pAp phosphatase activity with a k_{cat}/K_m value of 5.3 × 10^6 $M^{-1}s^{-1}$ (Table 5), comparable to that for 3-mer ssDNA (Table 4). TTHA0118 also degraded cAMP and cyclic GMP (cGMP), forming 5′-AMP and 5′-GMP, respectively, as a product (data not shown). H-prune, belonging to RecJ-like family II, is known to have cAMP phosphodiesterase activity (D'Angelo *et al*., 2004). However, the degrading activity of TTHA0118 was very low—the k_{cat}/K_m values for cAMP and cGMP were 2.5 and 6.7 $M^{-1}s^{-1}$, respectively (Table 5). Thus, the phosphohydrolase activity of TTHA0118 against 3′-phosphorylated mononucleotides was thought to be

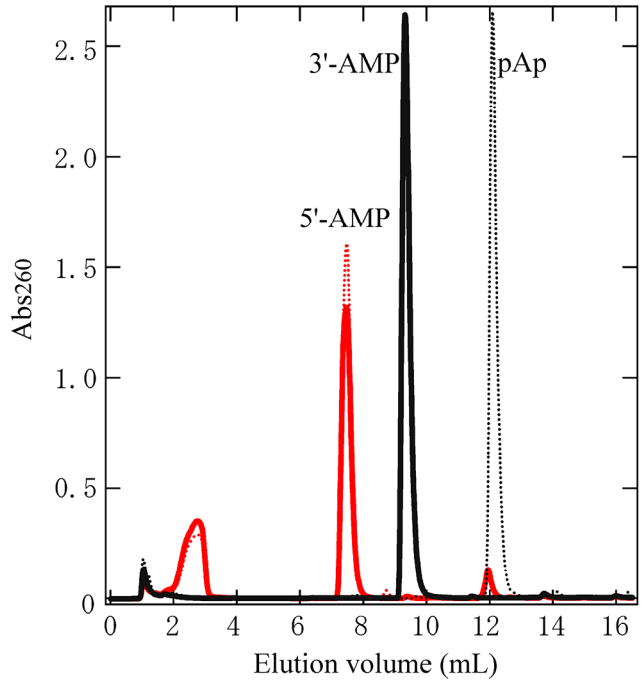

FIGURE 17. HPLC profile of the products in TTHA0118 pAp phosphatase activity. Elution profile of the product of pAp catalyzed by TTHA0118 (red solid line), a pAp control mixture (black dotted line), a 5′-AMP (red dotted line) control mixture, and 3′-AMP control mixture (black solid line). The enzyme reaction mixture was prepared as described under "Experimental procedures". Control mixture was prepared without TTHA0118.

TABLE 5. Kinetic constants for pAp, cAMP, and cGMP hydrolase activity of TTHA0118 and Mpn140[a].

Substrate	TTHA0118[b]			Mpn140[b]		
	K_m[c] (μM)	k_{cat}[c] (s^{-1})	k_{cat}/K_m ($M^{-1}s^{-1}$)	K_m (μM)	k_{cat} (s^{-1})	k_{cat}/K_m ($M^{-1}s^{-1}$)
pAp	1.8×10	9.5×10	5.3×10^{6}	3.2×10	7.5×10^{-1}	2.3×10^{4}
cAMP	1.4×10^{3}	3.5×10^{-3}	2.5	ND[d]	ND	ND
cGMP	2.4×10^{3}	1.6×10^{-2}	6.7	ND	ND	ND

[a]Assays were performed at pH 7.5 as described under "Experimental procedures".
[b]The reaction was performed in the presence of 5 mM $MgCl_2$.
[c]K_m and k_{cat} were determined from a nonlinear regression analysis.
[d]ND indicates not determined.

specific for pAp.

***Enzymatic Activity of Mpn140*:** Mpn140 degraded short ssDNAs and ssRNAs more efficiently than long ones in $MnCl_2$ in a 5′-3′ directed manner as well as did TTHA0118 and ttRecJ (Fig. 7, Table 4). Both k_{cat} and K_m values of Mpn140 were much lower than those of TTHA0118 (e.g. the value of k_{cat} and K_m for 6-mer ssDNA in the presence of $MnCl_2$ was 1.2×10^{-2} versus 9.1 s^{-1}, and 1.5 versus 2.8×10^2 μM). The metal dependence of Mpn140 differed between 6-mer and 11-mer ssDNA. For 6-mer ssDNA, the presence of Mg^{2+}, Ca^{2+}, Co^{2+}, and Zn^{2+} resulted in approximately 400%, 410%, 0%, and 0%, respectively, of the k_{app} observed in the presence of Mn^{2+}, and approximately 0%, 0%, 160%, and 0%, respectively, for 11-mer ssDNA. For 6-mer ssDNA and ssRNA exonuclease activity, Mg^{2+} was a more effective activating factor than Mn^{2+} and other *Mycoplasma* nucleases (Table 2, Bendjennat *et a*l., 1997). In the absence of metal ions, the k_{app} values for 6-mer and 11-mer ssDNAs were 380% and 150%, respectively, of the k_{app} values in the presence of Mn^{2+}. The respective activities were decreased to about 39% and 3.1% by adding 5 mM EDTA. Therefore, some metal ions were presumably bound to the purified Mpn140 strongly. Mpn140 was observed to have a high k_{cat}/K_m value (2.3×10^4 $M^{-1}s^{-1}$) for pAp phosphatase activity similar to TTHA0118 (Table 5).

***Growth of the Δttha0118 strain in CS medium*:** I disrupted the chromosomal *ttha0118* gene by insertion of a kanamycin resistance gene to determine the function of TTHA0118 in *T. thermophilus* cells. Wild-type and Δ*ttha0118* strains were cultivated in TT medium (rich medium) or CS medium (minimal essential medium). Comparing bacterial counts at 21 h after incubation from 1.5×10^5 cells/mL, disruption of *ttha0118*

caused slower growth in the CS medium (7.3×10^8 cells/mL) than in the TT medium (5.9×10^9 cells/mL) as shown in Fig. 18A. This suggested that Δ*ttha0118* strain was an auxotroph. Further, although the bacterial counts at 21 h incubation in TT plate were almost the same between the wild-type and Δ*ttha0118* strains, the colonies of Δ*ttha0118* strain were significantly smaller than those of the wild strain (Fig. 18B), similar to the Δ*orn* mutant from *Streptomyces griseus* and *Pseudomonas putida* (Ohnishi *et al*., 2000; Zhang *et al*., 2004), which suggested that the Δ*ttha0118* strain grew more slowly than did the wild strain in not only in the CS culture but also in the TT culture.

However, in the presence of mononucleotide mixtures or nucleoside mixtures, which are neutral and can pass through the cellular membrane, in the CS medium, the Δ*ttha0118* strain grew faster (3.2×10^9 or 3.9×10^9 cells/mL, respectively, Fig. 18A) than in the absence of these compounds. Furthermore, in the presence of cysteine in the CS medium, the Δ*ttha0118* strain grew faster (2.3×10^9 cells/mL, Fig. 18A).

***DNA microarray*:** I compared the Δ*ttha0118* strain to the wild strain to determine expression changes in the early log phase (cell density, 7×10^8 cells/mL) in the CS medium using a DNA microarray system (Affymetrix GeneChip). Among all of the 2,349 genes on the array, the expression levels of 54 genes differed more than 2-fold between the wild-type and Δ*ttha0118* strains. These genes are classified into several groups according to their functions (Tables 6 and 7). For the Δ*ttha0118* strain, the expressions of 29 genes were suppressed (Table 6), whereas 25 genes were activated (Table 7). Of the 29 downregulated genes in the Δ*ttha0118* mutant, five genes (TTHA310, TTHA311, TTHA312, TTHA1763, and TTHA1942) coded for cytochrome c oxidase-related protein and the molybdopterin oxidoreductase membrane subunit,

A

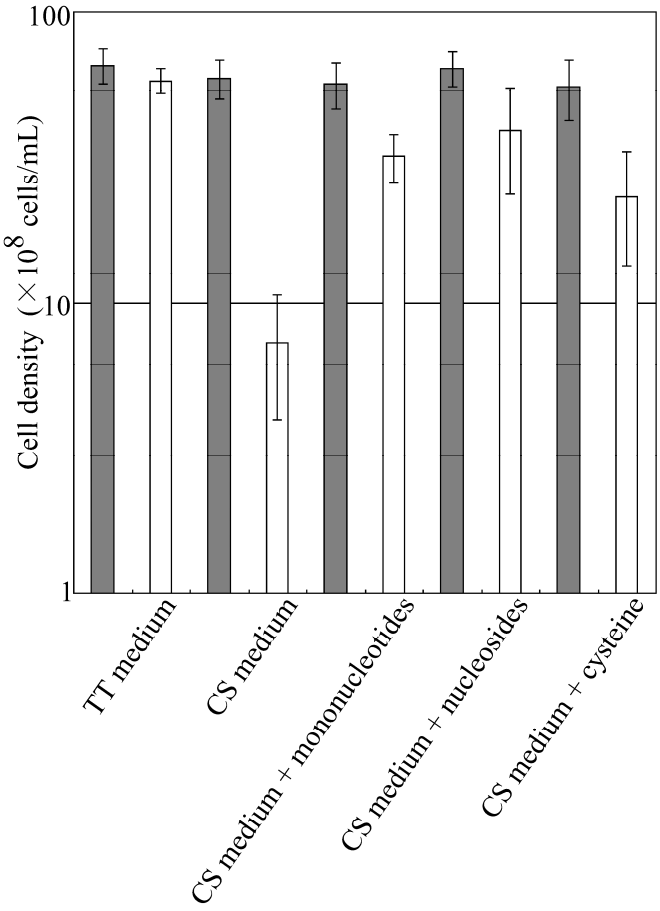

B

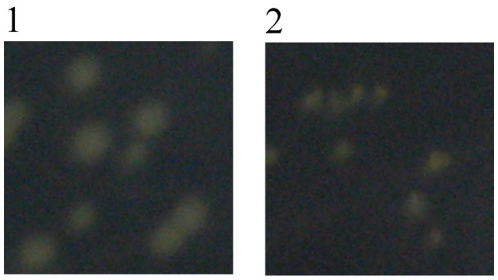

FIGURE 18. Phenotype of Δ*ttha0118* strain. *A*, Cell density of wild (gray columns) and Δ*ttha0118* (white columns) *T. thermophilus* HB8 in liquid TT or CS medium in the absence or presence of 0.1 mM mononucleotides, nucleosides, or cysteine. The cell density shown as arithmetical means ± standard deviation for four independent experiments. *B*, Slow growth of Δ*ttha0118* strain in the TT plate. The typical colonies of wild strain (panel 1) and Δ*ttha0118* strain (panel 2) in TT plate are photographed after 21 h incubation at 70°C.

TABLE 6. Subset of genes downregulated in Δ*ttha0118* strain.

Gene	Fold	Function	Product
ttha0310	0.263	Electron transport	Cytochrome c oxidase assembly factor (CtaA) + Protoheme IX farnesyltransferase (CtaB)
ttha0311	0.411	Electron transport	Cytochrome caa3 oxidase subunit IIc
ttha0312	0.387	Electron transport	Cytochrome caa3 oxidase subunit I (polypeptide I + III)
ttha1763	0.469	Electron transport	Molybdopterin oxidoreductase membrane subunit
ttha1942	0.209	Electron transport	Putative cytochrome c oxidase assembly protein
ttha0829	0.388	Metabolism	Putative acetoin utilization protein, acetoin dehydrogenase
ttha1329	0.405	Metabolism	Glutamine synthetase
ttha1973	0.469	DNA metabolism	Chromosomal replication initiator protein DnaA
ttha0819	0.403	Transporter	Sodium/solute symporter
ttha1137	0.474	Transporter	Major facilitator superfamily transporter
ttha1436	0.456	Transporter	ABC-type transporter, ATP-binding protein
tthb083	0.333	Transporter	Sugar ABC transporter, permease protein
ttha1137	0.390	Cell division	GTP-binding protein Era
ttha1498	0.380	Translation factor	Elongation factor G (EF-G-2)
ttha0118	0.054	This study	This study
ttha0285	0.437	Hypothetical protein	Hypothetical protein
ttha0494	0.498	Hypothetical protein	Hypothetical protein
ttha0592	0.494	Hypothetical protein	Hypothetical protein
ttha0816	0.283	Hypothetical protein	Hypothetical protein
ttha0820	0.446	Hypothetical protein	Hypothetical protein
ttha0988	0.453	Hypothetical protein	Hypothetical protein
ttha1627	0.329	Hypothetical protein	Hypothetical protein
ttha1760	0.424	Hypothetical protein	Hypothetical protein
ttha1761	0.373	Hypothetical protein	Hypothetical protein
ttha1762	0.380	Hypothetical protein	Hypothetical protein
ttha1765	0.471	Hypothetical protein	Hypothetical protein
tthb157	0.261	Hypothetical protein	Hypothetical protein
tthb158	0.384	Hypothetical protein	Hypothetical protein
tthb162	0.481	Hypothetical protein	Hypothetical protein

Only ORFs with a *P* value <0.05 by *t*-test have been listed.
Only ORFs with a fold change of <0.5 for the Δ*ttha0118* strain versus wild strain have been listed.

TABLE 7. Subset of genes upregulated in Δ*ttha0118* strain.

Gene	Fold	Function	Product
ttha1111	2.27	Stress response	Alternative ATP-dependent protease La (Lon protease)
ttha1489	2.16	Stress response	Chaperone protein DnaJ
ttha1490	2.24	Stress response	GrpE protein (HSP-70 cofactor)
ttha1491	2.48	Stress response	Chaperone protein DnaK (HSP70)
ttha1621	2.36	Stress response	Heat shock protein, class I
ttha0241	2.13	Metabolism	Oxidoreductase, short-chain dehydrogenase/reductase family
ttha1212	2.16	Metabolism	Acetolactate synthase, small subunit (ilvN)
ttha1213	2.07	Metabolism	Acetolactate synthase, large subunit
tthb101	2.65	Metabolism	Phytoene synthase
ttha1162	2.09	DNA metabolism	Excisionase domain protein
tthc001	2.60	DNA metabolism	Putative RepA protein
ttha0596	2.32	Transporter	ABC transporter solute-binding protein
ttha1418	2.49	Electron transport	Putative cytochrome c
tthb099	3.14	Transcriptional regulator	Transcriptional regulator, Crp family
ttha0109	2.28	Other function	ATP-dependent RNA helicase
ttha0135	2.13	Other function	MutT/nudix family protein
ttha1726	2.76	Other function	S-layer repressor
ttha0030	2.02	Hypothetical protei	Hypothetical protein
ttha0036	2.22	Hypothetical protein	Hypothetical protein
ttha0702	2.10	Hypothetical protein	Hypothetical protein
ttha0772	19.6	Hypothetical protein	Hypothetical protein
ttha0773	9.71	Hypothetical protein	Hypothetical protein
ttha1147	2.04	Hypothetical protein	Hypothetical protein
ttha1214	2.62	Hypothetical protein	Hypothetical protein
tthc005	2.25	Hypothetical protein	Hypothetical protein

Only ORFs with a *P* value <0.05 by *t*-test have been listed.
Only ORFs with a fold change of >2.0 for the Δ*ttha0118* strain versus wild strain have been listed.

which are involved in electron transport. Further, the GTP-binding protein Era (TTHA0120) was suppressed. Of the 25 upregulated genes, I found several genes that are typically associated with stress response. TTHA1489, TTHA1490, TTHA1491, and TTHA1621 are chaperone/cochaperone proteins, while TTHA1111 is a stress-induced protease.

Discussion

The homolog protein His-tagged YtqI from *B. subtilis* degraded 3-mer oligoribonucleotides more efficiently than long ones probably in a 3′-5′ directed manner akin to YhaM (Oussenko *et al*., 2002) and pAp. YtqI also complements the Δ*orn* mutant and Δ*cysQ* mutant in *E. coli* (Mechold *et al*., 2007).

In this study, I purified TTHA0118 and Mpn140 and characterized their physiochemical properties and enzyme activities. All these three proteins have 5′-3′ exonuclease activities. TTHA0118 and Mpn140 hydrolyzed short ssDNA and ssRNA preferentially, but ttRecJ did not show any such dependence on substrate length. The K_m values of TTHA0118 were greater than those of ttRecJ and Mpn140, while the electrophoretic mobility shift assay showed that *T. thermophilus* SSB did not enhance the binding activity for ssDNA of TTHA0118 (data not shown).

I showed that TTHA0118 and Mpn140 have not only oligoribonuclease activity but also oligodeoxyribonuclease such as Orn (Mechold *et al*., 2006) and Sfn (Nguyen *et al*., 2000). For 5-mer ssDNA and 5-mer ssRNA, the k_{cat}/K_m values of Sfn were 1.7×10^4 and 4.1×10^4 $M^{-1}s^{-1}$ (Nguyen *et al*., 2000, the k_{cat} values were 2.5×10^{-2} s^{-1} and 6.5×10^{-2} s^{-1}, and the K_m values were 1.5 μM andn1.6 μM, respectively). The values are similar to those of TTHA0118 and Mpn140 for 6-mer oligonucleotides. Oligonucleotides are thought to be formed by other endonucleases and exonucleases. TTHA0118 hydrolyzes the oligonucleotides to mononucleotides. When the crystal structure of the monomer BF3670 was compared with that of cd-ttRecJ, the root mean square deviation (r.m.s.d.) was 4.3 Å, which showed that the BF3670 structure was comparatively similar to the cd-ttRecJ structure. However, the number of highly

conserved residues whose side chains could interact with the backbone of nucleic acids in BF3670 (Arg105 and Arg291) is very low as compared with that of ttRecJ (Arg110, Asn273, Arg277, Asn307, Arg310, Gln311, Arg350, and Arg370). Moreover, the C-terminal length of the exopolyphosphatase-related protein is shorter than that of ttRecJ, and exopolyphosphatase-related proteins do not have the OB-domain. Thus, the length dependence of the exonuclease may be attributed to the number of residues whose side chains could interact with the backbone of nucleic acids and the rest to the C-terminal OB domain (Figs. 3 and 19).

TTHA0118 and Mpn140 also had high pAp phosphatase activity. pAp is known to act as a competitive inhibitor of many enzymes (Klaassen and Boles, 1997; Schneider *et al*., 1998; Dichtl *et al*., 1997). This is because high concentrations of pAp are toxic for cells, leading to the desirability of a mechanism to control the concentration. In beta and gamma Proteobacteria, Actinobacteria, CysQ (pAp phosphatase) is considered to control the pAp concentration (Hatzios *et al*., 2008). In Firmicutres, Bacterioidetes, Chlorobi, delta subdivision of Proteobacteria, Crenachaeota, and Euryarchaeota, which do not have CysQ, the exopolyphosphatase-related protein may degrade pAp for the control of pAp concentration.

While the supply of cysteine increased the doubling time of the Δ*ytqI B. subtilis* mutant in MOPS minimal medium, the complementary effects of nucleotides and nucleosides were not investigated (Mechold *et al*., 2007). Growth analysis in CS medium in the presence or absence of nucleotides, nucleosides, or cysteine suggested the possibility that TTHA0118 degrades short nucleic acids to produce mononucleotides for nutrients and pAp for concentration control *in vivo*. The Δ*ttha0118* strain grew much

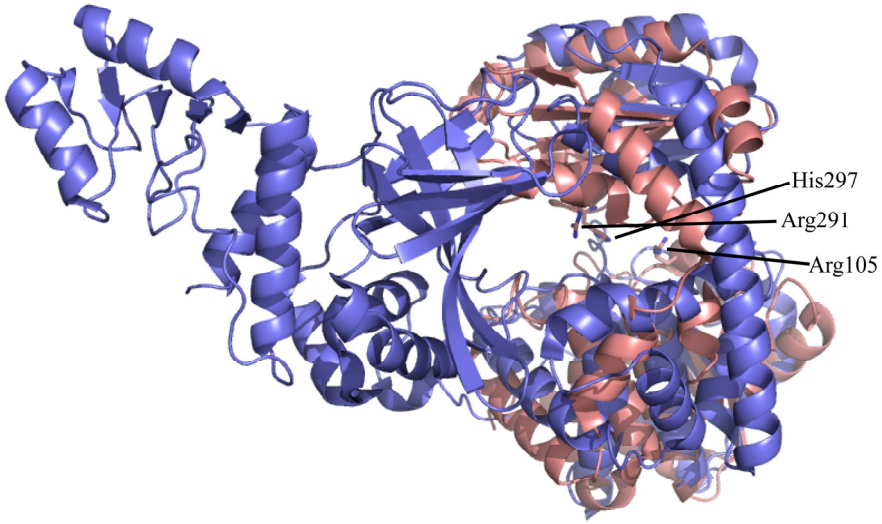

FIGURE 19. Overlap of the BF3670 structure (pink, PDB ID: 3DMA) and ttRecJ (blue, PDB ID: 2ZXO). The figure was produced with the LSQKAB program. Side chains of the possible residues for ssDNA and ssRNA binding are shown as stick forms. His297 in the DHHA1 motif is included.

slower than did the wild strain in the CS medium, and the difference in the transcriptional profiles of these strains was compared using DNA microarray. Heat shock proteins, which were upregulated in the Δ*ttha0118* strain, are also referred to as stress proteins; their upregulation is sometimes described more generally as part of the stress response involved in starvation (Werner-Washburne *et al*., 1989; Wu *et al*., 2004). Correspondingly, growth analysis with the Δ*ttha0118* mutant showed that disruption of *ttha0118* caused starvation. The enzyme cytochrome c oxidase, which was downregulated in the Δ*ttha0118* mutant, is a large transmembrane protein complex found in bactria, and is the last enzyme in the respiratory electron transport chain. Era is a membrane-associated GTP-binding protein, which has an essential role in cell growth and division in *E. coli* (Gollop and March, 1991). The downregulation of the expression of these genes is implicated in the delay of growth in the Δ*ttha0118* strain. In Tables 7 and 8, there are no genes listed that are involved in nucleotide metabolism or the direct assimilation of cysteine. It is possible that there were no changes in the transcription levels for these genes.

The amino acid sequence of *M. pneumoniae* Mpn140 shows a 24% identity match with TTHA0118 (Fig. 3B). *M. pneumoniae* is a common agent of respiratory infections, including pharyngitis and tracheobronchitis, in humans (Waldo and Krause, 2006; Waites and Talkington, 2004). Neither the genes nor the enzymes for the *de novo* biosynthesis of nucleic acid precursors, including purines and pyrimidines, in *Mycoplasma* (Himmelreich *et al*., 1996; Pollack *et al*., 1997; Razin, 1978) or in similar other parasites (McGugan *et al*., 2007; Joshi and Dwyer, 2007) have been identified. These species are thought to be completely dependent upon their host for the supply of these nucleic acid precursors while genomic sequence analyses of a number of

Mycoplasma species have identified novel enzymes associated with salvage pathways for the biosynthesis of nucleic acids from nucleotides (Himmelreich *et al*., 1996; Wang *et al*., 2001; Westberg *et al*., 2004). The identification of intracellular, extracellular, and membrane-associated nuclease activities in a number of *Mycoplasma* species suggests the involvement of nucleases in a variety of cellular processes (Minion *et al*., 1993; Bendjennat *et al*., 1997; Jarvill-Taylor *et al*., 1999; Schmidt *et al*., 2007). *Mycoplasma* nucleases are thought to play a metabolic role in the production of nucleotide substrates from host or microbial nucleic acids released through natural and induced cell death. Mpn140 is a polycistronic transcriptional unit with Mpn141 (major adhesin P1 protein) and Mpn142 (cytoadherence-related B/C protein) (Waldo and Krause, 2006), and these homolog proteins (MG190, MG191, and MG192) in *Mycoplasma genitalium* may be composed of polycistronic operons. This study showed Mpn140 has oligo(deoxy)ribonuclease activity and pAp phosphatase activity. Therefore, I hypothesize that Mpn140 hydrolyzes small ssDNA and ssRNA in human respiratory tracts and produces precursors for nucleic acids for themselves.

In summary, exopolyphosphatase-related proteins would function to produce mononucleotides and to control pAp concentration (Fig. 20). Considering these functions and the physiological distribution of exopolyphosphatase-related proteins, they might fulfill the function of Orn and CysQ. The short nucleotides and pAp will be accumulated in the deletion mutant of *exopolyphosphatase-related protein*.

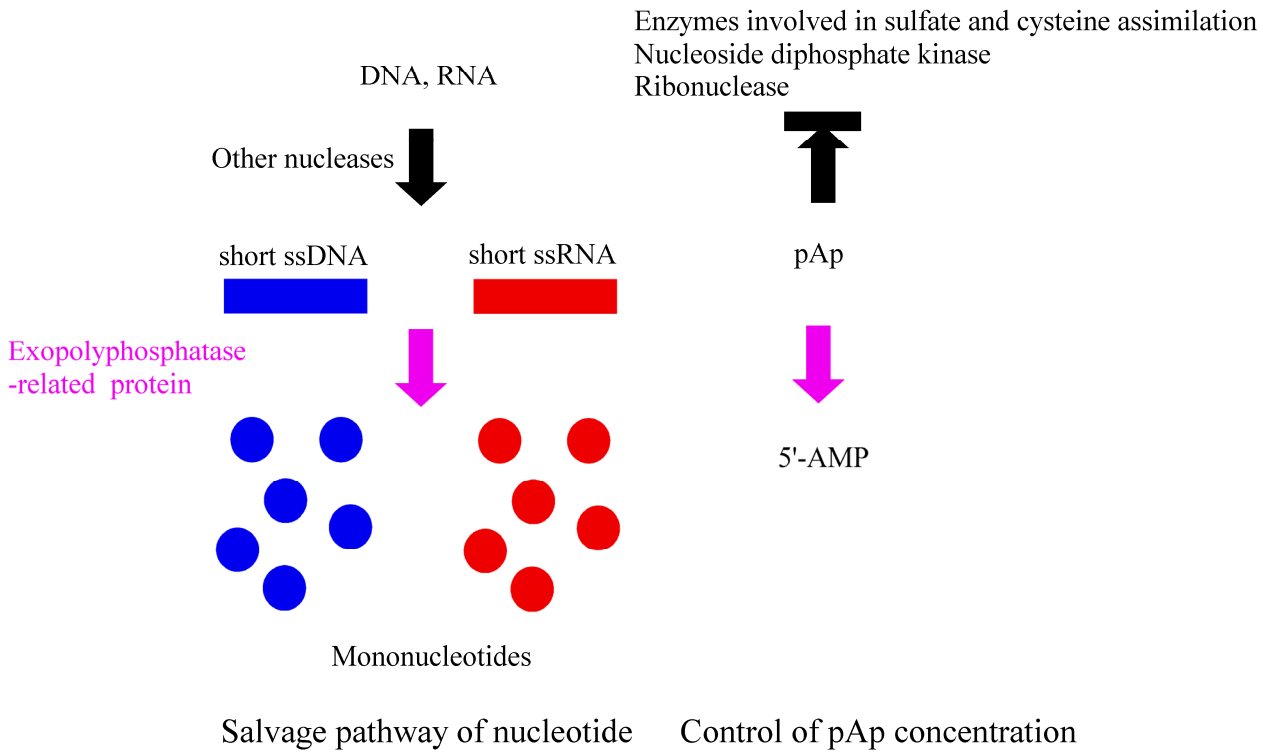

FIGURE 20. Overview of functions of exopolyphosphatase-related protein.

Comprehensive discussion

In chapter I, I determined the crystal structures of intact RecJ alone and in complex with Mg^{2+} and with Mn^{2+}. The structural analysis and characterization of the OB domain revealed the high specificity of RecJ for ssDNA. The presence of two Mn^{2+} ions in RecJ-Mn^{2+} complex structure suggested that RecJ cleaves ssDNA using a two-metal-ion mechanism in the catalytic reaction. Furthermore, the direct interaction between RecJ and SSB suggested that these two proteins function in close coordination with one another in DNA repair and recombination systems.

In chapter II, I showed the exopolyphosphatase-related proteins had 5'-3' exonuclease activity for short ssDNA and short ssRNA and pAp phosphatase activity in the presence of divalent cations. *In vivo* analysis of the gene disruptant suggested that this protein produces mononucleotides by degrading nucleic acids and controls pAp concentration.

These results in chapters I and II suggest that the difference in substrate specificity arising from the OB domain is correlated with the functional difference between RecJ and exopolyphosphatase-related proteins. These findings must be useful for the studies of other exonucleases.

References

Adams, P. D., Grosse-Kunstleve, R. W., Hung, L. W., Ioerger, T. R., McCoy, A. J., Moriarty, N. W., Read, R. J., Sacchettini, J. C., Sauter, N. K., and Terwilliger, T. C. (2002) *PHENIX*: building new software for automated crystallographic structure determination. *Acta Crystallogr. A* **58,** 1948–1954.

Andreeva, N., Kulakovskaya, T., Sidorov, I., Karpov, A., and Kulaev, I. (1998) Purification and properties of polyphosphatase from *Saccharomyces cerevisiae* cytosol. *Yeast* **14,** 383–390.

Aravind, L. and Koonin, E. V. (1998) A novel family of predicted phosphoesterases includes *Drosophila* prune protein and bacterial RecJ exonuclease. *Trends Biochem. Sci.* **23,** 17–19.

Baker, N. A., Sept, D., Joseph, S., Holst, M. J., and McCammon, J. A. (2001) Electrostatics of nanosystems: application to microtubules and the ribosome. *Proc. Natl. Acad. Sci. U. S. A.* **98,** 10037–10041.

Beese, L. S. and Steitz, T. A. (1991) Structural basis for the 3'-5' exonuclease activity of *Escherichia coli* DNA polymerase I: a two metal ion mechanism. *EMBO J.* **10,** 25–33.

Bendjennat, M., Blanchard, A., Loutfi, M., Montagnier, L., and Bahraoui, E. (1997) Purification and characterization of *Mycoplasma penetrans* Ca^{2+}/Mg^{2+}-dependent endonuclease. *J. Bacteriol.* **179,** 2210–2020.

Bochkarev. A. and Bochkareva, E. (2004) From RPA to BRCA2: lessons from single-stranded DNA binding by the OB-fold. *Curr. Opin. Struct. Biol.* **14,** 36–42.

Brünger, A. T., Adams, P. D., Clore, G. M., DeLano, W. L., Gros, P., Grosse-Kunstleve, R. W., Jiang, J. S., Kuszewski, J., Nilges, M., Pannu, N. S., Read, R. J., Rice, L. M., Simonson, T., and Warren, G. L. (1998) Crystallography & NMR system: A new software suite for macromolecular structure determination. *Acta Crystallogr. D* **54,** 905–921.

Burdett, V., Baitinger, C., Viswanathan, M., Lovett, S. T., and Modrich, P. (2001) *In vivo* requirement for RecJ, ExoVII, ExoI and ExoX in methyl-directed mismatch repair *Proc. Natl. Acad. Sci. U. S. A.* **98,** 6765–6770.

Cadman, C. J. and McGlynn, P. (2004) PriA helicase and SSB interact physically and functionally. *Nucleic Acids Res.* **32,** 6378–6387.

Ceska, T. A., Sayers, J. R., Stier, G., and Suck, D. (1996) A helical arch allowing single-stranded DNA to thread through T5 5'-exonuclease. *Nature* **382,** 90–93.

Collaborative Computational Project, No. 4. (1994) The CCP4 suite: programs for protein crystallography. *Acta Crystallogr. D* **50,** 760–763.

Courcelle, J. and Hanawalt, P. C. (1999) RecQ and RecJ process blocked replication forks prior to the resumption of replication in UV-irradiated *Escherichia coli*. *Mol. Gen. Genet.* **262**, 543–551.

Cooper, D. L., Lahue, R. S., and Modrich, P. (1993) Methyl-directed mismatch repair is bidirectional. *J. Biol. Chem.* **268,** 11823–11829.

Dabrowski, S., Olszewski, M., Piatek, R., and Kur, J. (2002) Novel thermostable ssDNA-binding proteins from *Thermus thermophilus* and *T. aquaticus*-expression and purification. *Protein Expr. Purif.* **26,** 131–138.

Dabrowski, S., Olszewski, M., Piatek, R., Brillowska-Dabrowska, A., Konopa, G., and Kur, J. (2002) Identification and characterization of single-stranded-DNA-binding proteins from *Thermus thermophilus* and *Thermus aquaticus* - new arrangement of binding domains. *Microbiology* **148,** 3307–3315.

Datta, A. K. and Niyogi, K. (1975) A novel oligoribonuclease of *Escherichia coli*. II. Mechanism of action. *J. Biol. Chem.* **250,** 7313–7319.

D'Angelo, A., Garzia, L., André, A., Carotenuto, P., Aglio, V., Guardiola, O., Arrigoni, G., Cossu, A., Palmieri, G., Aravind, L., and Zollo, M. (2004) Prune cAMP phosphodiesterase binds nm23-H1 and promotes cancer metastasis. *Cancer Cell* **5,** 137–149.

Dianov, G., Sedgwick, B., Daly, G., Olsson, M., Lovett, S. T., and Lindahl, T. (1994) Release of 5'-terminal deoxyribose-phosphate residues from incised abasic sites in DNA by the *Escherichia coli* RecJ protein. *Nucleic Acids Res.* **22,** 993–998.

Dichtl, B., Stevens, A., and Tollervey, D. (1997) Lithium toxicity in yeast is due to the inhibition of RNA processing enzymes. *EMBO J.* **6,** 7184–7195.

Eggington, J. M., Haruta, N., Wood, E. A., and Cox, M. M. (2004) The single-stranded DNA-binding protein of *Deinococcus radiodurans*. *BMC Microbiol.* **4,** 2.

Feng, W. Y. and Hays, J. B. (1995) DNA structures generated during recombination initiated by mismatch repair of UV-irradiated nonreplicating phage DNA in *Escherichia coli*: requirements for helicase, exonucleases, and RecF and RecBCD functions. *Genetics* **140,** 1175–1186.

Finn, R. D., Tate, J., Mistry, J., Coggil, P. C., Sammut, S. J., Hotz, H. R., Ceric, G., Forslund, K., Eddy, S. R., Sonnhammer, E. L., and Bateman, A. (2008) The Pfam protein families database. *Nucleic Acids Res.* **36,** 281–288.

Friedberg, E.C., Walker, G. C., and Siede, W. (1995) *DNA Repair and Mutagenesis* (American Society of Microbiology, Washington, DC).

Ghosh, S. and Deutscher, M. P. (1999) Oligoribonuclease is an essential component of the mRNA decay pathway. *Proc. Natl. Acad. Sci. U. S. A* **96,** 4372–4377.

Glusker, J. P. (1991) Structural aspects of metal liganding to functional groups in proteins. *Adv. Protein Chem.* **42,** 1–76.

Gollop, N. and March, P. E. (1991) A GTP-binding protein (Era) has an essential role in growth rate and cell cycle control in *Escherichia coli*. *J. Bacteriol.* **173,** 2265–2270.

Han, E. S., Cooper, D. L., Persky, N. S., Sutera, V. A., Whitaker, Jr. R. D., Montello, M. L., and Lovett, S. T. (2006) RecJ exonuclease: substrates, products and interaction with SSB. *Nucleic Acids Res.* **34,** 1084–1091.

Hashimoto, Y., Yano, T., Kuramitsu, S., and Kagamiyama, H. (2001) Disruption of *Thermus thermophilus* genes by homologous recombination using a thermostable kanamycin-resistant marker. *FEBS Lett.* **506,** 231–234.

Hatzios, S. K., Iavarone, A. T., and Bertozzi, C. R. (2008) Rv2131c from *Mycobacterium tuberculosis* is a CysQ 3'-phosphoadenosine-5'-phosphatase. *Biochemistry* **47,** 5823–5831.

Himmelreich, R., Hilbert, H., Plagens, H., Pirkl, E., Li, B. C., and Herrmann, R. (1996) Complete sequence analysis of the genome of the bacterium *Mycoplasma pneumoniae*. *Nucleic Acids Res.* **24,** 4420–4449.

Hosfield, D. J., Mol, C. D., Shen, B., and Tainer, J. A. (1998) Structure of the DNA repair and replication endonuclease and exonuclease FEN-1: coupling DNA and PCNA binding to FEN-1 activity. *Cell* **95,** 135–146.

Huang, C. Y., Hsu, C. H., Sun, Y. J., Wu, H. N., and Hsiao, C. D. (2006) Complexed crystal structure of replication restart primosome protein PriB reveals a novel single-stranded DNA-binding mode. *Nucleic Acids Res.* **34,** 3878–3886.

Jarvill-Taylor, K. J., VanDyk, C., and Minion, F. C. (1999) Cloning of mnuA, a membrane nuclease gene of *Mycoplasma pulmonis*, and analysis of its expression in *Escherichia coli*. *J. Bacteriol.* **181,** 1853–1860.

Kim, Y., Eom, S. H., Wang, J., Lee, D. S., Suh, S. W., and Steitz, T. A. (1995) Crystal structure of *Thermus aquaticus* DNA polymerase. *Nature* **376,** 612–616.

Klaassen, C. D. and Boles, J. W. (1997) Sulfation and sulfotransferases 5: the importance of 3'-phosphoadenosine 5'-phosphosulfate (PAPS) in the regulation of sulfation. *FASEB J.* **11,** 404–418.

Kovall, R. A. and Matthews, B. W. (1999) Type II restriction endonucleases: structural, functional and evolutionary relationships. *Curr. Opin. Chem. Biol.* **3,** 578–583.

Kowalczykowski, S. C. (2000) Initiation of genetic recombination and

recombination-dependent replication. *Trends Biochem. Sci.* **25,** 156–165.

Krause, A., Nicodème, P., Bornberg-Bauer, E., Rehmsmeier, M., and Vingron, M. (1999) WWW access to the SYSTERS protein sequence cluster sets. *Bioinformatics* **15,** 262–263.

Kuramitsu, S., Hiromi, K., Hayashi, H., Morino, Y., and Kagamiyama, H. (1990) Pre-steady-state kinetics of *Escherichia coli* aspartate aminotransferase catalyzed reactions and thermodynamic aspects of its substrate specificity. *Biochemistry* **29,** 5469–5476.

Laskowski, R. A., McArthur, M. W., Moss, D. S., and Thornton, J. M. (1993) "PROCHECK: a program to check the stereochemical quelity of protein structures. *J. Appl. Crystallogr.* **26,** 283–291.

Leiros, I., Timmins, J., Hall, D. R., and McSweeney, S. (2005) Crystal structure and DNA-binding analysis of RecO from *Deinococcus radiodurans*. *EMBO J.* **24,** 906–918.

Liu, J. H., Chang, T. W., Huang, C. Y., Chen, S. U., Wu, H. N., Chang, M. C., and Hsiao, C. D. (2004) Crystal structure of PriB, a primosomal DNA replication protein of *Escherichia coli*. *J. Biol. Chem.* **279,** 50465–50471.

Lohman, T. M. and Ferrari, M. E. (1994) *Escherichia coli* single-stranded DNA-binding protein: multiple DNA-binding modes and cooperativities. *Annu. Rev. Biochem.* **63,** 527–570.

Lopper, M., Holton, J. M., and Keck, J. L. (2004) Crystal structure of PriB, a component of the *Escherichia coli* replication restart primosome. *Structure* **12,** 1967–1975.

Lovett, S. T. and Kolodner, R. D. (1989) Identification and purification of a single-stranded-DNA-specific exonuclease encoded by the *recJ* gene of *Escherichia coli*. *Proc. Natl. Acad. Sci. U. S. A.* **86,** 2627–2631.

Lu, D. and Keck, J. L. (2008) Structural basis of *Escherichia coli* single-stranded DNA-binding protein stimulation of exonuclease I. *Proc. Natl. Acad. Sci. U. S. A.* **105,** 9169–9174.

Jones, T. A., Zou, J. Y., Cowan, S. W., and Kjeldgaard, M. (1991) Improved methods for building protein models in electron density maps and the location of errors in these models. *Acta Crystallogr. A* **47,** 110–119.

Joshi, M. B. and Dwyer, D. M. (2007) Molecular and functional analyses of a novel class I secretory nuclease from the human pathogen, *Leishmania donovani*. *J. Biol. Chem.* **282,** 10079–10095.

Makharashvili, N., Koroleva, O., Bera, S., Grandgenett, D. P., and Korolev, S. (2004) A

novel structure of DNA repair protein RecO from *Deinococcus radiodurans*. *Structure* **2,** 1881–1889.

Matthews, B. W. (1968) Solvent content of protein crystals. *J. Mol. Biol.* **33,** 491–497.

McGugan, G. C. Jr, Joshi, M. B., and Dwyer, D. M. (2007) Identification and biochemical characterization of unique secretory nucleases of the human enteric pathogen, *Entamoeba histolytica*. *J. Biol. Chem.* **282,** 1789–1802.

Mechold, U., Ogryzko1, V., Ngo, S. and Danchin, A. (2006) Oligoribonuclease is a common downstream target of lithium-induced pAp accumulation in *Escherichia coli* and human cells. *Nucleic Acids Res.* **34,** 2364–2373.

Mechold, U., Fang, G., Ngo, S., Ogryzko, V., and Danchin, A. (2007) YtqI from *Bacillus subtilus* has both oligoribonuclease and pAp-phosphatase activity. *Nucleic Acids Res.* **35,** 4552–4561.

Minion, F. C., Jarvill-Taylor, K. J., Billings, D. E., and Tigges, E. (1993) Membrane-associated nuclease activities in mycoplasmas. *J. Bacteriol.* **175,** 7842–7847.

Mol, C. D., Kuo, C. F., Thayer, M. M., Cunningham, R. P., and Tainer, J. A. (1995) Structure and function of the multifunctional DNA-repair enzyme exonuclease III. *Nature* **374,** 381–386.

Murzin, A. G. (1993) OB (oligonucleotide/oligosaccharide binding)-fold: common structural and functional solution for non-homologous sequences. *EMBO J.* **12,** 861–867.

Neuwald, A. F., Krishnan, B. R., Brikun, I., Kulakauskas, S., Suziedelis, K., Tomcsanyi, T., Leyh, T. S., Berg, D. E. (1992) *cysQ*, a gene needed for cysteine synthesis in *Escherichia coli* K-12 only during aerobic growth. *J. Bacteriol.* **174,** 415–425.

Nguyen, L. H., Erzberger, J, P., Root, J., and Wilson, D. M. III. (2000) The human homolog of *Escherichia coli* Orn degrades small single-stranded RNA and DNA oligomers. *J. Biol. Chem.* **275,** 25900–25906.

Niyogi, S. K. and Datta, A. K. (1975) A novel oligoribonuclease of *Escherichia coli*. I. Isolation and properties. *J. Biol. Chem.* **250,** 7307–7312.

Nowotny, M., Gaidamakov, S. A., Crouch, R. J., and Yang, W. (2005) Crystal structures of RNase H bound to an RNA/DNA hybrid: substrate specificity and metal-dependent catalysis. *Cell* **121,** 1005–1016.

Ohnishi, Y., Nishiyama, Y., Sato, R., Kameyama, S., Horinouchi, S. (2000) An oligoribonuclease gene in *Streptomyces griseus*. *J. Bacteriol.* **182,** 4647-4653.

Otwinowski, Z. and Minor, W. (1997) *Methods Enzymol.* **276,** 307–326.

Oussenko I. A., Sanchez, R., Bechhofer, D. H. (2002) *Bacillus subtilis* YhaM, a member

of a new family of 3'-to-5' exonucleases in gram-positive bacteria. *J. Bacteriol.* **184,** 6250–6259.

Perry, J. J., Yannone, S. M., Holden, L. G., Hitomi, C., Asaithamby, A., Han, S., Cooper, P. K., Chen, D. J., and Tainer, J. A. (2006) WRN exonuclease structure and molecular mechanism imply an editing role in DNA end processing. *Nat. Struct. Mol. Biol.* **13,** 414–422.

Pollack, J. D., Williams, M. V., and McElhaney, R. N. (1997) The comparative metabolism of the mollicutes (mycoplasmas): the utility for taxonomic classification and the relationship of putative gene annotation and phylogeny to enzymatic function in the smallest free-living cells. *Crit. Rev. Microbiol.* **23,** 269–354.

Pollack, J. D., Myers, M. A., Dandekar, T., and Herrmann, R. (2002) Suspected utility of enzymes with multiple activities in the small genome Mycoplasma species: the replacement of the missing "household" nucleoside diphosphate kinase gene and activity by glycolytic kinases. *OMICS* **6,** 247–258.

Rajman, L. A. and Lovett, S. T. (2000) A thermostable single-strand DNase from *Methanococcus jannaschii* related to the RecJ recombination and repair exonuclease from *Escherichia coli*. *J. Bacteriol.* **182,** 607–612.

Razin, S. (1978) The mycoplasmas. *Microbiol. Rev.* **42,** 414–470.

Schärer, O. D. (2003) Chemistry and biology of DNA repair. *Angew. Chem. Int. Ed. Engl.* **42,** 2946–2974.

Schmidt, J. A., Browning, G. F., and Markham, P. F. (2007) *Mycoplasma hyopneumoniae* mhp379 is a Ca^{2+}-dependent, sugar-nonspecific exonuclease exposed on the cell surface. *J. Bacteriol.* **189,** 3414–3424.

Schneider, B., Xu, Y. W., Janin, J., Véron, M., and Deville-Bonne, D. (1998) 3'-Phosphorylated nucleotides are tight binding inhibitors of nucleoside diphosphate kinase activity. *J. Biol. Chem.* **273,** 28773–28778.

Sharma, R., Rao, D. N. (2009) Orchestration of *Haemophilus influenzae* RecJ exonuclease by interaction with single-stranded DNA-binding protein. *J. Mol. Biol.* **385,** 1375–1396.

Shereda, R. D., Bernstein, D. A., and Keck, J. L. (2007) A central role for SSB in *Escherichia coli* RecQ DNA helicase function. *J. Biol. Chem.* **282,** 19247–19258.

Shereda, R. D., Reiter, N. J., Butcher, S. E., and Keck, J. L. (2009) Identification of the SSB Protein Binding Site on *E. coli* RecQ Reveals a Conserved Surface for Binding SSB Protein's C Terminus. *J. Mol. Biol.* **386,** 612–625.

Shinkai, A., Kira, S., Nakagawa, N., Kashihara, A., Kuramitsu, S., and Yokoyama, S. (2007) Transcription activation mediated by a cyclic AMP receptor protein from *Thermus thermophilus* HB8. *J. Bacteriol.* **189,** 3891–3901.

Shioi, S., Ose, T., Maenaka, K., Shiroishi, M., Abe, Y., Kohda, D., Katayama, T., and Ueda, T. (2005) Crystal structure of a biologically functional form of PriB from *Escherichia coli* reveals a potential single-stranded DNA-binding site. *Biochem. Biophys. Res. Commun.* **326,** 766–776.

Suck, D. and Oefner, C. (1986) Structure of DNase I at 2.0 Å resolution suggests a mechanism for binding to and cutting DNA. *Nature* **321,** 620–625.

Sutera, V. A. Jr, Han, E. S., Rajman, L. A., and Lovett, S. T. (1999) Mutational analysis of the RecJ exonuclease of *Escherichia coli*: identification of phosphoesterase motifs. *J. Bacteriol.* **181,** 6098–6102.

Tammenkoski, M., Moiseev, V. M., Lahti, M., Ugochukwu, E., Brondijk, T. H., White, S. A., Lahti, R., and Baykov, A. A. (2007) Kinetic and mutational analyses of the major cytosolic exopolyphosphatase from *Saccharomyces cerevisia*e. *J Biol Chem.* **282,** 9302–9311

Theobald, D. L., Mitton-Fry, R. M., and Wuttke, D. S. (2003) Nucleic acid recognition by OB-fold proteins. *Annu. Rev. Biophys. Biomol. Struct.* **32,** 115–133.

Thompson, J. D., Higgins, D. G., and Gibson, T. J. (1994) CLUSTAL W: improving the sensitivity of progressive multiple sequence alignment through sequence weighting, position-specific gap penalties and weight matrix choice. *Nucleic Acids Res.* **22,** 4673–4680.

Ugochukwu, E., Lovering, A. L., Mather, O. C., Young, T. W., and White, S. A. (2007) The crystal structure of the cytosolic exopolyphosphatase from *Saccharomyces cerevisiae* reveals the basis for substrate specificity. *J. Mol. Biol.* **371,** 1007–1021.

Vagin, A. and Teplyakov, A. (1997) *MOLREP*: an Automated Program for Molecular Replacement. *J. Appl. Cryst.* **30,** 1022–1025.

Viswanathan, M., Burdett, V., Baitinger, C., Modrich, P., and Lovett, S. T. (2001) Redundant exonuclease involvement in *Escherichia coli* methyl-directed mismatch repair. *J. Biol. Chem.* **276**, 31053–31058.

Waites, K. B. and Talkington, D. F. (2004) *Mycoplasma pneumoniae* and its role as a human pathogen. *Clin. Microbiol. Rev.* **17,** 697–728.

Wakamatsu, T., Nakagawa, N., Kuramitsu, S., and Masui, R. (2008) Structural basis for different substrate specificities of two ADP-ribose pyrophosphatases from *Thermus thermophilus* HB8. *J. Bacteriol.* **190,** 1108–1117.

Waldo, R. H. III and Krause, D. C. (2006) Synthesis, stability, and function of

cytadhesin P1 and accessory protein B/C complex of *Mycoplasma pneumoniae*. *J. Bacteriol.* **188,** 569–575.

Wang, L., Westberg, J., Bolske, G., and Eriksson, S. (2001) Novel deoxynucleoside-phosphorylating enzymes in mycoplasmas: evidence for efficient utilization of deoxynucleosides. *Mol. Microbiol.* **42,** 1065–1073.

Westberg, J., Persson, A., Holmberg, A., Goesmann, A., Lundeberg, J., Johansson, K. E., Pettersson, B., and Uhlén, M. (2004) The genome sequence of Mycoplasma mycoides subsp. mycoides SC type strain PG1T, the causative agent of contagious bovine pleuropneumonia (CBPP). *Genome Res.* 14, 221–227

Werner-Washburne, M., Becker, J., Kosic-Smithers, J., and Craig, E. A. (1989) Yeast Hsp70 RNA levels vary in response to the physiological status of the cell. *J. Bacteriol.* **171,** 2680–2688.

Wold, M. S. (1997) Replication protein A: a heterotrimeric, single-stranded DNA-binding protein required for eukaryotic DNA metabolism. *Annu. Rev. Biochem.* **66,** 61–92.

Wu, J., Zhang, N., Hayes, A., Panoutsopoulou, K., and Oliver, S. G. (2004) Global analysis of nutrient control of gene expression in *Saccharomyces cerevisiae* during growth and starvation. *Proc. Natl. Acad. Sci. U. S. A.* **101,** 3148–3153.

Yanyushin, M. F., del Rosario, M. C., Brune, D. C., and Blankenship, R. E. (2005) New class of bacterial membrane oxidoreductases. *Biochemistry* **44,** 10037–10045.

Yamagata, A., Kakuta, Y., Masui, R., and Fukuyama, K. (2002) The crystal structure of exonuclease RecJ bound to Mn^{2+} ion suggests how its characteristic motifs are involved in exonuclease activity. *Proc. Natl. Acad. Sci. U. S. A.* **99,** 5908–5912.

Yamagata, A., Masui, R., Kakuta, Y., Kuramitsu, S., and Fukuyama, K. (2001) Overexpression, purification and characterization of RecJ protein from *Thermus thermophilus* HB8 and its core domain. *Nucleic Acids Res.* **29,** 4617–4624.

Yokoyama, S., Hirota, H., Kigawa, T., Yabuki, T., Shirouzu, M., Terada, T., Ito, Y., Matsuo, Y., Kuroda, Y., Nishimura, Y., Kyogoku, Y., Miki, K., Masui, R., and Kuramitsu, S. (2000) Structural genomics projects in Japan. *Nat. Struct. Biol.* **7,** 943–945.

Zhang, X., Zhu, L., and Deutscher, M. P. (1998) Oligoribonuclease is encoded by a highly conserved gene in the 3'-5' exonuclease superfamily. *J. Bacteriol.* **180,** 2779–2781.

Zhang, X. X., Lilley, A. K., Bailey, M. J., and Rainey, P. B. (2004) Functional and phylogenetic analysis of a plant-inducible oligoribonuclease (*orn*) gene from an indigenous *Pseudomonas* plasmid. *Microbiology* **150,** 2889–2898.

Acknowledgements

I would like to express my great appreciation to Professor Seiki Kuramitsu and Drs. Ryoji Masui and Noriko Nakagawa for their guidance and many valuable discussions. I also would like to express my great appreciation to Professors Satoru Kawamura and Akihiro Ogura and Katsuyuki Tanizawa for their critical advices in this study. I am grateful to Yoshiaki Kitamura, Yuka Nonaka, and Toshi Arima for their help in the X-ray data collections. I wish to thank Miwa Ohmori for support on the DNA microarray analysis. I wish to thank Hirohumi Ohmori for DNA sequencing. I wish to thank Dr. Naoto Ohtani for providing us with the genome of *M. pneumoniae* M129. Finally, I thank my colleagues in Kuramitsu laboratory for their kind help in this study.

List of publications

1. Yoshikawa. S., Arai, R., Kinoshita, Y., Uchikubo-Kamo, T., Wakamatsu, T., Akasaka, R., Masui, R., Terada, T., Kuramitsu, S., Shirouzu, M., and Yokoyama, S. (2007) Structure of archaeal glyoxylate reductase from *Pyrococcus horikoshii* OT3 complexed with nicotinamide adenine dinucleotide phosphate. *Acta Crystallogr. D* **63,** 357–365.
2. Agari. Y., Sato, S., Wakamatsu, T., Bessho, Y., Ebihara, A., Yokoyama, S., Kuramitsu, S., and Shinkai, A. (2007) X-ray crystal structure of a hypothetical Sua5 protein from *Sulfolobus tokodaii* strain 7. *PROTEINS: Structure, Function, and Bioinformatics*. **70,** 1108–1111.
3. Wakamatsu. T., Nakagawa, N., Kuramitsu, S., and Masui, R. (2008) Structural basis for different substrate specificities of two ADP-ribose pyrophosphatases from *Thermus thermophilus* HB8. *J. Bacteriol.* **190,** 1108–1117.
4. Kondo. N., Nishikubo, T., Wakamatsu, T., Ishikawa, H., Kuramitsu, S., and Masui, R. (2008) Insights into different dependence of dNTP triphosphohydrolase on metal ion species from intracellular ion concentrations in *Thermus thermophilus*. *Extremophiles* **12,** 217–223.
5. Tomoike, F., Wakamatsu, T., Nakagawa, N., Kuramitsu, S., and Masui, R. Crystal structure of *Thermus thermophilus* HB8 TTHA1606, a conserved hypothetical protein that may be a DNA-binding protein. *PROTEINS: Structure, Function, and Bioinformatics*. Accepted.